Experimental studies and computational exploration on the 2-amino-5-(2-methoxyphenyl)-1,3,4-thiadiazole as novel corrosion inhibitor for mild steel in acidic environment

A. Attou, M. Tourabi, A. Benikdes, O. Benali, H.B. Ouici, F. Benhiba, A. Zarrouk, Charafeddine Jama, Fouad Bentiss

Experimental studies and computational exploration on the 2-amino-5-(2-methoxyphenyl)-1,3,4-thiadiazole as novel corrosion inhibitor for mild steel in acidic environment

A. Attou [a], M. Tourabi [b], A. Benikdes [c], O. Benali [c], H.B. Ouici [c], F. Benhiba [d,e], A. Zarrouk [e,*], C. Jama [f], F. Bentiss [b,f,*]

[a]*Department of Chemistry, Faculty of Sciences, University Dr Moulay Tahar, Saïda, Algeria*
[b]*Laboratory of Catalysis and Corrosion of Materials, Faculty of Sciences, Chouaib Doukkali University, PO Box 20, M-24000 El Jadida, Morocco*
[c]*Laboratory of Chemistry: Synthesis, Properties and Applications, University Dr Moulay Tahar, Saïda, Algeria*
[d] *Laboratory of Separation Processes, Faculty of Sciences, University Ibn Tofail, Kenitra, Morocco.*
[e]*Laboratory of Materials, Nanotechnology and Environment, Faculty of Sciences, Mohammed V University, Av. Ibn Battouta, PO Box 1014 Agdal-Rabat, Morocco*
[f]*Univ. Lille, CNRS, INRAE, Centrale Lille, UMR 8207, - UMET - Unité Matériaux et Transformations, F-59000 Lille, France*

** Corresponding authors.*
E-mail address: azarrouk@gmail.com (A. Zarrouk)
fbentiss@gmail.com (F. Bentiss)

ABSTRACT

In the present research, a new 1,3,4-thiadiazole derivative, namely the 2-amino-5-(2-methoxyphenyl)-1,3,4-thiadiazole (5-AMT) was synthesized and investigated as corrosion inhibitor for mild steel (M-steel) in molar hydrochloric acid medium. The experimental studies such as weight loss, potentiodynamic polarization (PDP), Linear polarization resistance (LPR) technique and electrochemical impedance spectroscopy (EIS) were performed in order to evaluate the corrosion protection performance of the tested compound. Based on the experimental outcomes, a protection degree of approximately 98 % was achieved exploiting 5×10^{-4} M of 5-AMT after 1 h of immersion at temperature 303 K. Additionally, PDP study highlighted that the investigated 1,3,4-thiadiazole is of mixed-kind inhibitor. Thermodynamic data from adsorption isotherms and activation energies were determined and discussed. It was shown that the adsorption of 5-AMT molecules fits Langmuir isotherm model. Furthermore, in order to characterize the M-steel surface and to comprehend the adsorption mechanism of 5-AMT, XPS analyses were accomplished. Computational studies by DFT and MD simulation were also conducted to correlate the protection properties and quantum chemical parameters of the investigated inhibitor.

Keywords: 1,3,4-Thiadiazole; Mild steel corrosion; Adsorption; XPS; Theoretical approach.

1. Introduction

Corrosion of metals and alloys is an ubiquitous phenomenon with huge economic impact, which affects many industrial sectors [1]. Preventing metals from corrosion not only has an economic benefit, but also protects the environment. Generally, organic inhibitors are known by their absorption on metal surfaces and form a thin protective film. The most effective organic compounds are those which carry heteroatoms with high electron density (P, S, N and O) or those containing aromatic ring, which are considered as centers of adsorption [2-6]. Indeed, several N-heterocyclic compounds, such as triazoles, oxadiazoles, benzimidazoles, pyrazoles, purines, pyrimidines, quinolones, etc… are well known as effective corrosion inhibitors for iron or steel in several aggressive media [5-7]. The high corrosion protection of these latter compounds is generally due to chelates formed with metals which act as a barrier thanks to the formation of protective film on the metal surface [1]. In particular, these thiadiazolic derivatives behave as good inhibitors against corrosion of M-steel and carbon steel [8-22], stainless steel [23-25], ductile iron [26], and copper [27-32]. At this time, the utilize of 1,3,4-thiadiazole derivatives as corrosion inhibitors rest limited. In this context, this work aims to investigate the 2-amino-5-(2-methoxyphenyl)-1,3,4-thiadiazole(5-AMT) as new corrosion inhibitor of M-steel in molar hydrochloric acid pickling environment. The 5-AMT compound was selected as an inhibitor based on two considerations. Firstly, it's easy and cheap to synthesis. Secondly, the existence of heteroatoms such as N, O and S, methoxy group and π-electron on the phenyl ring in its structure are important structural features through which inhibitor can easily adsorbed on the metal surface, promoting therefore an effective protection.

The inhibitory efficacy of 2-amino-5- (2-methoxyphenyl) -1,3,4-thiadiazole (5-AMT) is first evaluated by means of gravimetry, and, by means of stationary electrochemical techniques the exploitation of the polarization curves as well as transient methods based on the measurement

of the electrochemical impedance and LPR technique. The effect of temperature on the behavior of the inhibitor against corrosion has also been studied in a temperature range from 303 to 333 K. Thermodynamic corrosion and inhibition parameters were also calculated and discussed. The nature of the film formed on the metal surface in the presence of the inhibitor has been characterized XPS. At the end of this study, we supplemented this work by a study the density functional theory and molecular dynamic simulation were exploited to better understand the structural and electronic effects in relation to the effectiveness of the protection. The use of all these experimental and theoretical approaches were used to better understand the mechanism of adsorption of this compound on the metal surface.

2. Experimental details

The investigated organic compound is 2-amino-5-(2-methoxyphenyl)-1,3,4-thiadiazole (5-AMT). The method of synthesis of the inhibitor under investigation was already described in the literature [33]. The molecular structure of 5-AMT is given in Fig. 1.

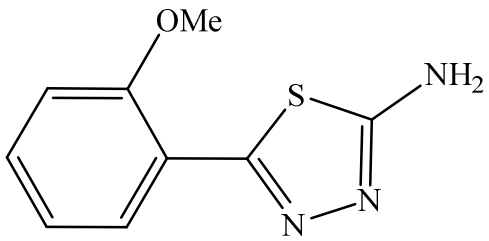

Fig. 1. Molecular structure of 2-amino-5-(2-methoxyphenyl)-1,3,4-thiadiazole (5-AMT).

The composition of the M-steel, the electrolytic solution (1 M HCl) as well as the description of different methods exploited in this work (weight loss and the electrochemical experiments) were detailed in our previous work [34].

X-ray photoelectron spectroscopy (XPS) spectra were recorded by a XPS KRATOS, AXIS Ultra^{DLD} spectrometer with the monochromatized Al-Kα X-ray source ($h\nu$ = 1486.6

eV) and an X-ray beam of around 1 mm. The analyser was operated in constant pass energy of 40 eV using an analysis area of approximately 700 µm × 300 µm. Charge compensation was applied to compensate for the charging effects that occurred during the analysis. The C 1s (285.0 eV) binding energy (BE) was used as internal reference. The spectrometer BE scale was initially calibrated against the Ag $3d_{5/2}$ (368.2 eV) level. Pressure was in the 10^{-10} torr range during the experiments. Quantification and simulation of the experimental photopeaks were carried out using CasaXPS software. Quantification took into account a non-linear Shirley background subtraction [35]. XPS analyses were practiced on pure 5-AMT and on 5-AMT steel surface. The M-steel sample (1 cm^2) was pre-treated by the same procedure as for the gravimetric test. After 6 h of immersion at 303 K, the carbon steel sheet was rinsed with acetone and ultra-pure water.

Various investigations have been carried out exploiting density functional theory (DFT) calculations in order to understand the effect of molecular structure on the protection efficiency of organic compounds [36]. This theoretical method has been exploited to correlate experimentally detected phenomena with the property of the electronic structure MT [37]. In this context, quantum chemical calculations of 5-AMT were done exploiting the Gaussian 09 software package [38]. In addition, DFT computations were performed via B3LYP and 6–31G (d, p) basis set in the gaseous phase [39]. The quantum chemical descriptors such as E_{HOMO}, E_{LUMO}, ΔE_{gap}, global hardness (η), global electronegativity (χ), fraction of electron transferred ΔN_{110}, electrophilic (ω) and nucleophilic (ε) indexes were exploited and calculated following the same procedure described by Benhiba et al. [40].

To estimate the interaction and adsorption behaviour of inhibitor molecules with the Fe (110) surface, Molecular Dynamics (MD) simulation method exploiting the Forcite module from Materials Studio 8 software was exploited according to [41,42]. The MD simulation was executed in a 32.270×32.270×34.134 $Å^3$ simulation box with periodic

boundary conditions, which was composed of the chemical species (5-AMT, $5H_3O^+ + 5Cl^- + 500\ H_2O$) and slab of Fe (110). The COMPASS force field has been exploited [43]. The MD simulation is performed with the Andersen thermostat at 303 K using NVT (canonical ensemble) with a simulation time of 100.0 ps and a time step of 1.0 fs [44].

3. Results and discussion

3.1. Potentiodynamic polarization (PDP) curves

Polarization curves (Tafel) for M-steel without and with 5-AMT in the electrolytic solution (1 M HCl) at 303 K after 1 h of immersion are grouped in Figs. 2a-b. The electrochemical parameters of corrosion potential (E_{corr}), corrosion current density (i_{corr}), cathodic Tafel slope (β_c), and anodic Tafel slope (β_a), obtained by Tafel extrapolation are shown in the Table 1. The corrosion current density (i_{corr}) values were used to compute the protection efficiency as follows:

$$\eta_{Tafel}(\%) = \frac{i_{corr} - i_{corr(i)}}{i_{corr}} \times 100 \qquad \text{(Eq. 1)}$$

where i_{corr} and $i_{corr(i)}$ are the corrosion current densities obtained in uninhibited and inhibited solutions, respectively.

It is evident from Fig. 2b that after the addition of 5-AMT both hydrogen evolution and metal dissolution reactions were retarded. By increasing the C_{inh} it is noted that the density values of the corrosion current decreased, which indicates that the inhibitor limits electrochemical reaction. In addition, we notice that when the C_{inh} increases, $\eta_{Tafel}(\%)$ also increases to reach a maximum of 98.68%, which is assigned to the fact that the quality of the 5-AMT inhibitive layer was improved, and more active sites were covered by 1,3,4-

thiadiazole molecules. The inhibition efficiency found by this technique allowed us to say that 5-AMT is an excellent inhibitor even at low concentration (0.1 mM).

From Table 1, it is noticed that the change in β_c values of the inhibited systems with respect to that of the uninhibited one is independent of inhibitor concentration, that is, there is no pattern in β_c values of the inhibited solution with respect to that of the blank as the concentration of 5-AMT is increased. This means that the kinetics of the cathodic reactions are not affected and the corrosion inhibition is by simple geometric blocking mechanism. However, a slight decrease in β_a value with increasing 5-AMT concentration is observed, suggesting that the investigated 1,3,4-thiadiazole derivative was first adsorbed onto the metal surface and stopped by simply blocking the reaction sites of the metal surface without touching the anodic reaction mechanism [34].

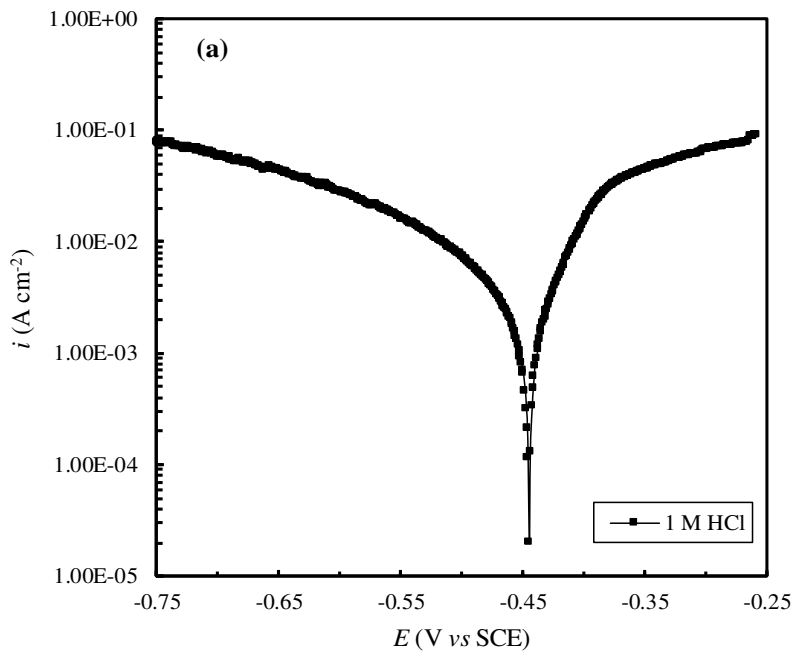

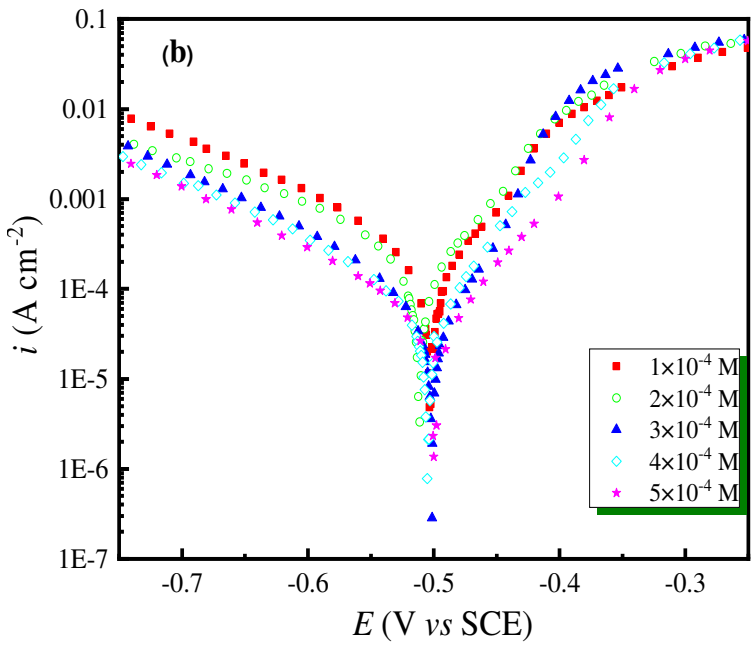

Fig. 2. PDP curve of M-steel in electrolytic medium (1 M HCl) (a) without and (b) with addition of of 5-AMT at diverse concentrations.

The corrosion potentials in the presence 5-AMT are divided slightly towards the cathodic values compared to the blank. It can be understood from the Table 1 values that 5-AMT shifts the corrosion potential (E_{corr}) towards cathodic direction and the potential shift is < 85 mV, confirms that inhibitor is a mixed type of protection behaviour [45]. It should be noted that for the anodic branch in the presence of 5-AMT and from a potential of -350 mV/SCE, the currents are greater than that of without 5-AMT inhibitor. This phenomenon is attributed to the desorption of inhibitor molecules adsorbed on the electrode surface [34].

Table 1

Electrochemical parameter and inhibition efficiency values for M-steel in electrolytic medium (1 M HCl) containing different concentrations of 5-AMT at 303 K.

C_{inh} (M)	$-E_{corr}$ (mV *vs* SCE)	$-\beta_c$ (mV dec^{-1})	β_a (mV dec^{-1})	i_{corr} (mA cm^{-2})	R_p (Ω cm^2)	η_{Tafel} (%)	η_{LPR} (%)
Blank	445	185	105	4.24	6.78	—	—
1×10^{-4}	503	167	85	0.32	66.43	92.45	89.79
2×10^{-4}	512	190	83	0.31	99.03	92.69	93.15

3×10^{-4}	502	150	80	0.086	231.87	97.97	97.08
4×10^{-4}	505	162	72	0.083	293.37	98.04	97.17
5×10^{-4}	500	148	70	0.056	392.98	98.68	98.27

3.2 LPR study

The polarization resistance, R_p, is determined by the inverse of the slope corresponding to the linear part of the curve $i = f(E)$ in the vicinity of E_{corr}. The corresponding data of R_p are given in the Table 1. It is apparent that by increasing inhibitor (5-AMT) concentration the values of R_p increase. The values of $\eta_{LPR}(\%)$, have been gathered in Table 1 and they are calculated by the following equation(Eq2):

$$\eta_{LPR}(\%) = \frac{R_{P(i)} - R_p}{R_{P(i)}} \times 100 \qquad \text{(Eq. 2)}$$

The results show that by increasing the concentration of inhibitor, $\eta_{LPR}(\%)$ increases and attains 98.27 % for 5×10^{-4} M. It can be noted that the corrosion inhibition efficiency calculated by the LPR and PDP methods are in reasonably agreement. However, these stationary techniques are insufficient to characterize complex mechanisms, involving several reaction stages and having different characteristic kinetics (which is often the case during inhibition processes). The use of AC impedance techniques then becomes essential. Among these techniques, electrochemical impedance spectroscopy occupies a more advanced place.

3.3 . AC impedance study

Figs. 3a and 3b present Nyquist and Bode plots obtained for M-steel in 1 M HCl solution with and without 5-AMT after 1 h of immersion at 303 K. Fig. 3a shows that the Nyquist plots present a non-ideal semicircle (a flat loop). This is attributed to the non-ideality and inhomogeneity of the metal surface [46]. The Nyquist plots represent the characteristic depressed semicircles with their centers lying under the real x-axis suggesting that the

electrochemical process is charge-transfer controlled. The corresponding Bode plots shown in Fig. 3b confirm the presence of only one constant time due to charge transfer phenomenon at the interface electrolyte/working electrode.

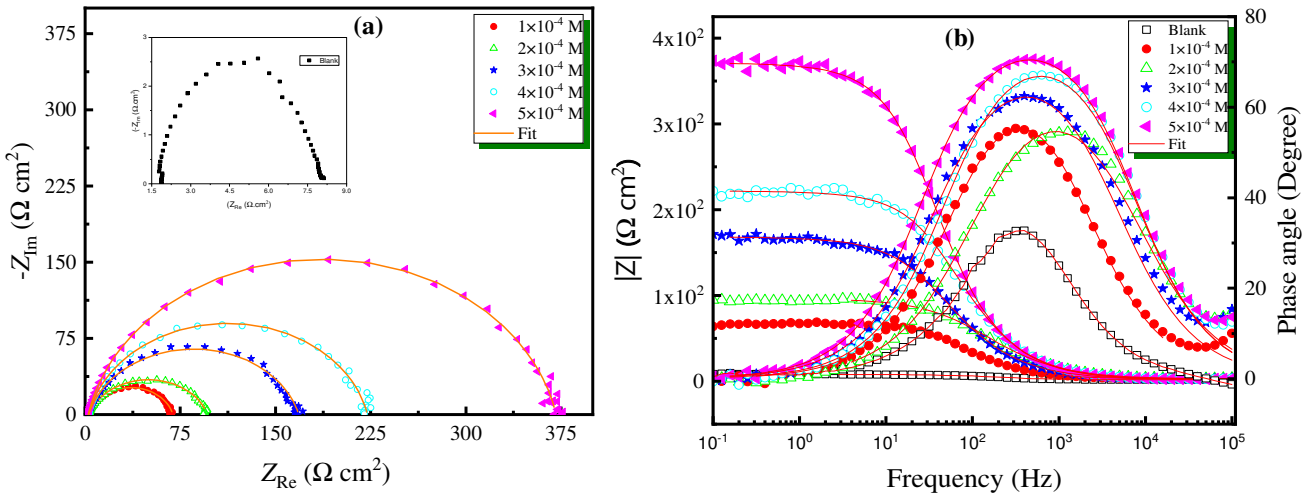

Fig. 3. (a) Nyquist and (b) Bode (modulus and phase) diagrams for M-steel interface in 1 M HCl medium without and with addition of diverse concentrations of 5-AMT at 303 K.

The impedance spectra in Fig. 3a shows that the semicircle diameter values increase with the increase of 5-AMT concentration. These outcomes are interpreted by the formation of a protective film on the metal surface via the adsorption of the inhibitor molecules [10]. The equivalent circuit shown in Fig. 4 allowed us to analyse the EIS data, this equivalent circuit is a modified Randel's circuit containing the R_s, which represents the uncompensated resistance of the electrolytic solution, and the R_p, which represents the polarization resistance. Herein, we have used a constant phase element (CPE) rather than an ideal double-layer capacitor (C_{dl}), to accurately model the frequency distribution response. Here, R_p contains two resistances ($R_p = R_{ct} + R_f$) which are the charge transfer resistance (R_{ct}) and the resistance of inhibitor film (R_f) formed on the metal surface in the presence of inhibitor [47]. On the other

hand, the CPE is substituted for the capacitive element. The impedance function of the CPE is given in Equation (Eq. 3) [47]:

$$Z_{\mathrm{CPE}} = Q^{-1}(\mathrm{i}\omega)^{-n} \qquad \text{(Eq. 3)}$$

where Z_{CPE}, Q, ω, n are respectively, the impedance of CPE, the coefficient of proportionality, the angular frequency and the measure of the phase shift. The description of this model is detailed in a previous work [10].

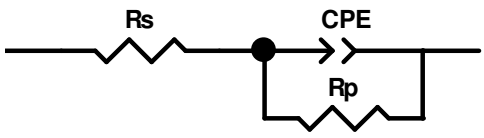

Fig. 4. Equivalent circuit used to fit the obtained impedance spectra for M-steel in the nonexistence and existence of 5-AMT.

The corrosion protection efficiency from the EIS measurements, $\eta_Z(\%)$, was calculated as according to equation 4, where $R_{p(i)}$ and R_p are the polarization resistance of M-steel electrode in the presence and the absence of the inhibitor, respectively.

$$\eta_Z(\%) = \frac{R_{P(i)} - R_p}{R_{P(i)}} \times 100 \qquad \text{(Eq. 4)}$$

The fitted results are presented in Table 2. The experimental plots and the fit lines indicates the chosen equivalent electrical circuits fit very well the experimental EIS diagrams (Fig. 3). It is also confirmed by the chi-square adjustment values (χ^2) which are around 10^{-3} (Table 2).

Table 2

Impedance data of M-steel in 1 M HCl containing different concentrations of 5-AMT

C_{inh} (M)	R_p (Ω cm^2)	$Q \times 10^4$ (s^n Ω^{-1} cm^{-2})	n	C_{dl} (μF cm^{-2})	τ (s)	χ^2	η_Z (%)
Blank	6.25	47.56	0.86	184.3	0.0011	0.009	—
1×10^{-4}	65.63	0.93	0.86	40.55	0.0027	0.009	90.47

2×10^{-4}	92.54	0.72	0.84	27.72	0.0026	0.010	93.25
3×10^{-4}	165.6	0.60	0.85	27.00	0.0044	0.012	96.22
4×10^{-4}	220.0	0.31	0.87	14.71	0.0032	0.006	97.16
5×10^{-4}	369.0	0.27	0.88	14.40	0.0053	0.006	98.30

From Table 2, we can see that the values of R_p are much higher when 5-AMT inhibitor is exploited in comparison to the electrolytic solution. The obtained result suggests that the presence of the molecules of the inhibitor at the metal-electrolyte interface limit the process of charge transfer from the metal surface to the solution. Moreover, one can see that when the concentration of inhibitor (5-AMT) in the solution increases the R_p values are even greater. On the other hand, due to the adsorption of 5-AMT at the interfaces, the C_{dl} values decrease which is attributed to an increase in the thickness of the electric double layer [48]. The values of n remain almost constant, indicating a small depression of the double layer capacitance of the loop [10]. The protection efficiency reaches a greatest value of 98.30 % at 5×10^{-4} M. The use of 1,3,4-thiadiazole derivatives as corrosion inhibitors has been discussed in several publications [8-32,49-51]. Table 3 shows the protection efficiency η(%) obtained exploiting EIS method of some 1,3,4-thiadiazole derivatives exploited as corrosion inhibitors of steel in a 1 M HCl medium. Such comparison shows that the protection efficiency η(%) of 5-AMT is higher and give evidence of the very good corrosion protection properties of 5-AMT.

Table 3

Corrosion protection efficiency for some 1,3,4-thiadiazole derivatives in 1 M HCl.

1,3,4-Thiadiazole derivative	Optimum concentration	Immersion time (h)	Temperature (K)	Metal	Protection efficiency [(a)] (%)
2-Amino-5-thiol-1,3,4-thiadiazole [10]	2×10^{-3} M	1	303	M-steel	91.2
5,5'-((1Z,1'Z)-(1,4-phenylenebis(methanylylidene))bis(azanylylidene))bis(1,3,4-thiadiazole-2-thiol) [14]	5×10^{-4} M	0.5	303	M-steel	87.6
5-Pentadecyl-1,3,4-thiadiazole-2(3H)-thione [15]	5×10^{-4} M	0.5	298	Carbon steel	93.0

2,5-Bis(2-pyridyl)-1,3,4-thiadiazole [17]	1.2×10^{-3} M	24	303	M-steel	93.5
2,5-Bis(3-pyridyl)-1,3,4-thiadiazole [17]	1.2×10^{-3} M	24	303	M-steel	96.5
2,5-Bis(4-pyridyl)-1,3,4-thiadiazole [17]	1.2×10^{-3} M	24	303	M-steel	86.6
APT [19]	40 ppm	0.5	308	M-steel	95.0
APT2 [19]	40 ppm	0.5	308	M-steel	96.8
APT-4 [19]	40 ppm	0.5	308	M-steel	92.7
PAT [19]	40 ppm	0.5	308	M-steel	98.6
2-Amino-5-phenyl-1,3,4-thiadiazole [20]	6×10^{-3} M	1	303	M-steel	88.6
2,5-Bis(phenyl)-1,3,4-thiadiazole [22]	1.5×10^{-4} M	24	303	M-steel	90.9
2,5-Bis(4-methoxyphenyl)-1,3,4-thiadiazole [22]	1.5×10^{-4} M	24	303	M-steel	97.9
2,5-Bis(4-methylphenyl)-1,3,4-thiadiazole [22]	1.5×10^{-4} M	24	303	M-steel	95.6
2,5-Bis(4-nitrophenyl)-1,3,4-thiadiazole [22]	1.5×10^{-4} M	24	303	M-steel	54.8
2,5-Bis(4-chlorophenyl)-1,3,4-thiadiazole [22]	1.5×10^{-4} M	24	303	M-steel	29.6
2-Amino-5-tert-butyl-1,3,4-thiadiazole [49]	2.1×10^{-5} M	0.5	298	Carbon steel	91.8
2-Amino-5-ethyl-1,3,4-thiadiazole [49]	2.1×10^{-5} M	0.5	298	Carbon steel	90.9
2-Amino-1,3,4-thiadiazole [49]	2.1×10^{-5} M	0.5	298	Carbon steel	78.1
1-MCTH [50]	1×10^{-4} M	24	303	M-steel	98.6
2,5-bis(4-dimethylaminophenyl)-1,3,4-thiadiazole [51]	5×10^{-4} M	24	303	M-steel	98.2
2,5-bis(4-dimethylaminophenyl)-1,3,4-thiadiazole [51]	5×10^{-4} M	24	303	M-steel	98.2
2-amino-5-(2-methoxyphenyl)-1,3,4-thiadiazole [this work]	5×10^{-4} M	1	303	M-steel	98.3

(a) The η(%) values were obtained by exploiting EIS method.

3.4. Gravimetric studies

3.4.1 Effect of 5-AMT concentration

Table 4 gives the corrosion rate (W_{corr}) of M-steel and the protection efficiency (η_{WL}) with and without of 5-AMT after 6h of immersion in 1 M HCl at 303 K. The η_{WL} values were obtained from the Eq. 5, where w_0 and w_i are the corrosion rate of M-steel without and with 5-AMT, respectively.

$$\eta_{WL}(\%) = \left(1 - \frac{w_i}{w_0}\right) \times 100 \qquad \text{(Eq. 5)}$$

The obtained results indicate that the protection ability of 5-AMT increase with the inhibitor concentration and achieve the highest efficiency value at a concentration of 5×10^{-4} M. Table 4 reveals that when the inhibitor concentration varies in the range of 1×10^{-4} to 3×10^{-4} M the efficiency of 5-AMT significantly increases. On the other hand, for higher concentrations, a slight increase can be observed. The efficiency of the inhibitor is a direct consequence of the covering and the formation of an organic film on the surface of the M-steel, which reduces the attack of the acid and the digestion of H_2 gaz. The easy adsorption of 5-AMT molecules may be due to the presence of π electrons in the phenyl group and non-binding electrons on the hetero-atoms (O, N and S) [52]. The results obtained with different methods are in good agreement and confirm the very good corrosion protection properties of 5-AMT. In order to evaluate the stability of the behavior of this compound, on a time scale, the electrochemical impedance measurements were carried out in 1 M HCl, in the absence and in the presence of this compound, after different immersion times in the next part

Table 4
Corrosion rate and protection efficiency of the system 5-AMT/M-steel in electrolytic solution.

C_{inh} (M)	W_{corr} (mg cm^{-2} h^{-1})	η_{WL} (%)
Blank	4.20	—
1×10^{-4}	0.58	86.19
2×10^{-4}	0.47	88.81
3×10^{-4}	0.21	95.00
4×10^{-4}	0.17	95.95
5×10^{-4}	0.084	98.00

3.4.2. Effect of immersion time

Immersion time is one of the main parameters considered during the study of the protection of corrosion [52-54], indeed it evaluates the stability of protection system over time. Fig. 5 shows the variation of η_{WL}(%) versus time of immersion in 1 M HCl solution containing 5×10^{-4} M of 5-AMT at 303 K. Better performance was obtained after 1 h of immersion with a value of 98% (Fig. 5). For a longer exposure time (24 h), our inhibitor (5-

AMT) always retains its high efficacy, which reaches a value of 97%. From the obtained results, we can say that there is a rapid formation and can be complete with a protective film on the surface of our substrate after 1 h of immersion. After this time, we notice that there is a very negligible diminution in the steadiness of the protective layer. This can be said during diffusion from side to side the protective interface / electrolytic layer and / or the desorption of the protective molecules. [55].

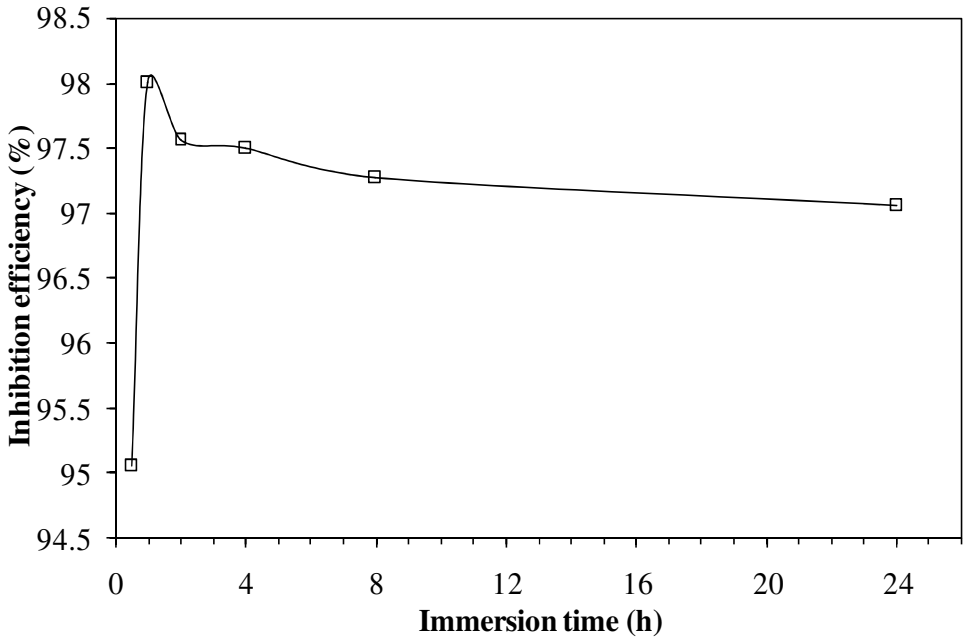

Fig. 5. η_{WL}(%) versus immersion time in 1 M HCl medium containing 5×10^{-4} M of 5-AMT at 303 K.

3.4.3. Temperature effect on the inhibitor adsorption

The temperature is considered, in the literature, among the most influencing factors on corrosion, in a very great majority of the cases, the exposure of a material in an aggressive solution to the high temperatures results in an appreciably homogeneous degradation on all the surface of the material. The effect of the temperature on the corrosion of the M-steel in the presence of the inhibitor was followed by mass loss evaluation. Table 5 presents the different

values of the corrosion rates as well as the corresponding inhibitory efficiencies in the temperature range 303-333 K. It shows that the corrosion rates increase with increasing temperature whether in the 5-AMT nonexistence or in the 5-AMT existence of the inhibitor molecules leading to a decrease of protection efficiency with the temperature. This is due to the fact that the protective film formed by the inhibitor molecules desorbs and becomes porous giving way to the diffusion of corrosive species responsible when the temperature increases [54-57].

Table 5
Influence of temperature on corrosion rate and protection efficiency for the system, M-steel / 1 M HCl / 5-AMT.

Temperature (K)	C_{inh} (M)	W_{corr} (mg cm^{-2} h^{-1})	η_{WL} (%)
303	Blank	4.20	—
	1×10^{-4}	0.58	86.19
	2×10^{-4}	0.47	88.81
	3×10^{-4}	0.21	95.00
	4×10^{-4}	0.17	95.95
	5×10^{-4}	0.084	98.00
313	Blank	4.70	—
	1×10^{-4}	2.30	51.06
	2×10^{-4}	0.77	83.61
	3×10^{-4}	0.37	92.13
	4×10^{-4}	0.27	94.25
	5×10^{-4}	0.18	96.17
323	Blank	8.20	—
	1×10^{-4}	5.00	39.02
	2×10^{-4}	2.30	75.60
	3×10^{-4}	0.67	91.83
	4×10^{-4}	0.55	93.20
	5×10^{-4}	0.40	95.12
333	Blank	14.14	—
	1×10^{-4}	8.50	39.88
	2×10^{-4}	4.50	68.17
	3×10^{-4}	3.00	78.78
	4×10^{-4}	1.50	89.39
	5×10^{-4}	0.72	94.90

However, the activation energy (E_a), enthalpy (ΔH_a), and entropy (ΔS_a) were estimated from the W_{corr}, as follows:

$$W_{\text{corr}} = A\exp\left(-\frac{E_{\text{a}}}{RT}\right) \quad \text{(Eq. 6)}$$

$$W_{\text{corr}} = \frac{RT}{Nh}\exp\left(\frac{\Delta S_{\text{a}}}{R}\right)\exp\left(-\frac{\Delta H_{\text{a}}}{RT}\right) \quad \text{(Eq. 7)}$$

where E_a, ΔH_a and ΔS_a are the activation parameters, A is pre-exponential factor, h is constant of Plank, N is number of Avogadro, R is the constant of ideal gaz, and T is the absolute temperature.

Figs. 6 and 7 show the variation of $\ln(W_{corr})$ and $\ln(W_{corr}/T)$ against $1000/T$ for M-steel electrode in 1 M HCl electrolyte in the absence and presence of diverse concentrations of 5-AMT. The activation parameters extracted from these two curves are collated in Table 6. The average difference between E_a and ΔH_a is approximately 2.6 kJ mol^{-1} for all cases. This indicates that the dissolution of M-steel takes place through an uni-molecular reaction.

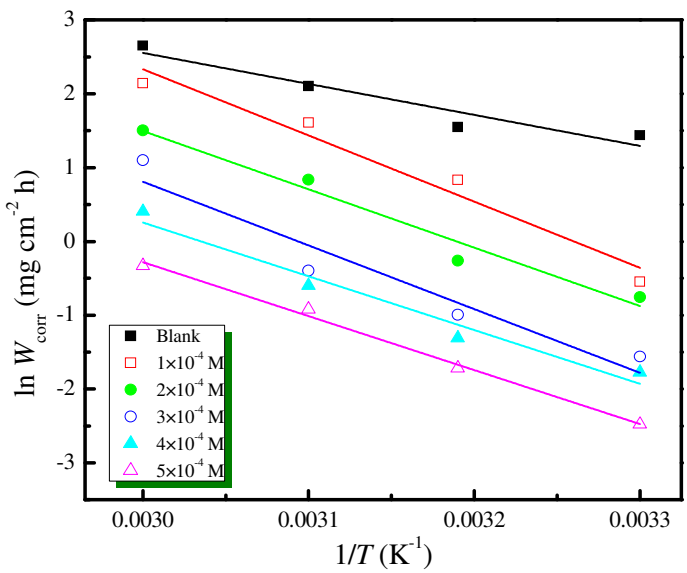

Fig. 6. $\ln W_{corr}$ *vs* $1/T$ for M-steel in 1 M HCl with and without of 5-AMT.

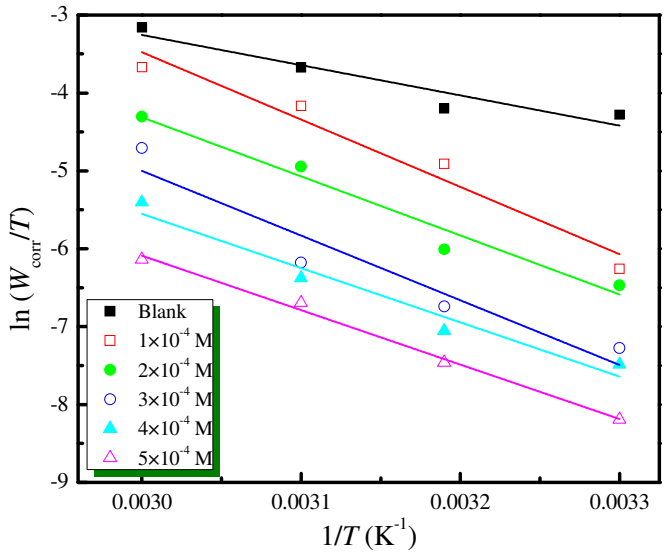

Fig. 7. ln(W_{corr} / T) *vs* 1/T for M-steel in 1 M HCl with and without of 5-AMT.

It was found that E_a values for systems containing 5-AMT vary in the range of 60.53 to 74.50 kJ mol^{-1} and are superior to blank (34.91 kJ mol^{-1}). The increase in E_a values after the addition of the inhibitor molecules indicates the formation of an energy barrier which is accompanied by the reduction in charge and mass transfer. These results are coherent with those reported in the literature, the decrease of protection efficiency with temperature is associated to higher E_a in presence of the inhibitor in comparison to E_a (blank) [58]. For the activation enthalpy (ΔH_a), the positive sign indicates the endothermic nature of the M-steel dissolving process [59,60]. On comparing the values of the entropy of activation (ΔS_a) in Table 6, it is clear that ΔS_a is more positive in presence of 5-AMT compared to free acid solution. Such variation is associated with the phenomenon of ordering and disordering of inhibitor molecules on the M-steel surface. The increased entropy of activation in the presence of inhibitor indicated that disorderness is increased on going from reactant to activated complex. This observation is in agreement with the findings of other workers [59,60]. This behaviour can also be explained as a result of the replacement process of water

molecules during adsorption of molecule inhibitor on the M-steel surface and therefore the increasing in entropy of activation was attributed to the increasing in solvent entropy [60].

Table 6

Activation parameters (E_a, ΔH_a and ΔS_a) for M-steel / 1 M HCl system containing 5-AMT.

Conc. (M)	E_a (kJ mol^{-1})	ΔH_a (kJ mol^{-1})	ΔS_a (J mol^{-1} K^{-1})
Blank	34.91	32.27	-127.8
1×10^{-4}	74.50	71.87	-10.85
2×10^{-4}	65.67	63.03	-44.29
3×10^{-4}	71.71	69.07	-31.90
4×10^{-4}	60.53	57.89	-70.04
5×10^{-4}	60.76	58.11	-73.83

3.4.3. Adsorption isotherm

To demonstrate the efficiency of inhibitors and to determinate the mechanism of the molecules action, adsorption isotherms are often exploited. In this part, the classical Langmuir adsorption isotherm is applied to describe the adsorption behavior of the 5-AMT, and the isotherm can be represented as:

$$\frac{C_{\text{inh}}}{\theta} = \frac{1}{K_{\text{ads}}} + C_{\text{inh}} \qquad \text{(Eq. 8)}$$

where K_{ads} and C_{inh} are the equilibrium constant of the adsorption process and is the concentration of 5-AMT, respectively. The standard free energy of adsorption (ΔG^{o}_{ads}) is related to K_{ads} according the following equation:

$$K_{\text{ads}} = (55.55)^{-1} e^{\left(\frac{-\Delta G^{o}_{\text{ads}}}{RT}\right)} \qquad \text{(Eq. 9)}$$

where R and T are the constant of ideal gas and the absolute temperature, respectively. The plots of C_{inh}/θ vs. C_{inh} show straight lines (Fig. 8) and the adsorption parameters were determined and are presented in Table 7. The deviation of the slopes from the unit can be

attributed to the interaction between the inhibitory molecules adsorbed, especially at high temperature (Table 7). Villamil et al. [62] proposed a modified Langmuir isotherm, which is given by following equation (Eq. 10):

$$\frac{C_{\text{inh}}}{\theta} = \frac{n}{K_{\text{ads}}} + nC_{\text{inh}} \qquad \text{(Eq. 10)}$$

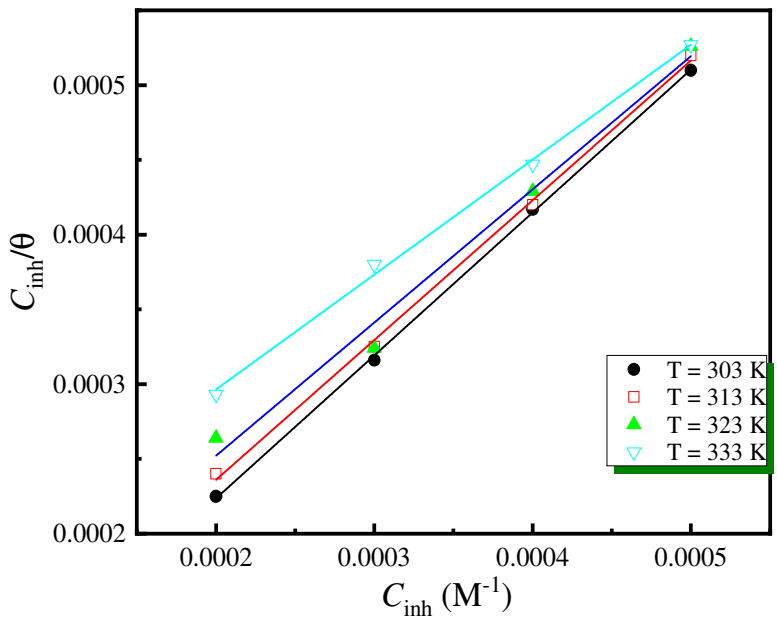

Fig. 8. Langmuir isotherm model for M-steel /1 M HCl / 5-AMT system.

Table 7
Parameters of adsorption for M-steel with 5-AMT in 1 M HCl.

Temperature (K)	R^2	Slope	K_{ads} (L mol^{-1})	$\Delta G^{\circ}_{\text{ads}}$ (kJ mol^{-1})	$\Delta H^{\circ}_{\text{ads}}$ (kJ mol^{-1})	$\Delta S^{\circ}_{\text{ads}}$ (J mol^{-1}K^{-1})
303	0.999	0.981	4.30×10^4	-36.99		
313	0.999	0.935	1.91×10^4	-36.10		
323	0.988	0.891	1.21×10^4	-36.02	-61.12	79.4
333	0.991	0.710	4.44×10^3	-34.37		

The obtained negative value of $\Delta G^{\circ}_{\text{ads}}$ indicates that the adsorbed layer is stable and the adsorption process onto the metal surface is spontaneous [10,63]. The nature of the interaction between 5-AMT and metal surface could be interpreted by three modes: physical adsorption, chemical adsorption or by complexation. The nature and charge of the metal (alloys), the type

of electrolytic solution and the chemical structure of the inhibitor are the essential parameters that influence these last three modes [64]. The values of ΔG^{o}_{ads} for the studied inhibitor varies between -36.99 kJ mol^{-1}and -34.37 kJ mol^{-1}, indicating therefore that the adsorption mechanism of 5-AMT on M-steel surface involves two types of interactions, predominant physisorption (ionic) and weak chemisorption (molecular) [63-65]. In fact, the adsorption of our inhibitor on the surface of M-steel in two different ways: either the 5-AMT molecules adsorb electrostatically on the part of the surface of the substrate covered with Cl^{-} ions through its protonated form and or that the 5-AMT molecules compete with acid anions for sites at the water overcast surface and the unshared electron pairs in heteroatoms (O, N and/or S) interact with d-orbitals of M-steel to provide a protective film.

The thermodynamic parameters ΔH^{o}_{ads} (variation of enthalpy) and ΔS^{o}_{ads} (variation of entropy) for the adsorption of 5-AMT on M-M-steel is given by the following equation:

$$\Delta G^{o}_{ads} = \Delta H^{o}_{ads} - T\ \Delta S^{o}_{ads} \qquad \text{(Eq. 11)}$$

The values of ΔG^{o}_{ads} were plotted versus temperature T (Fig. 9). From equation 11 and Fig. 9 we can calculate the two adsorption parameters (ΔS^{o}_{ads} and ΔH^{o}_{ads}), their values are gathered in the Table 7.

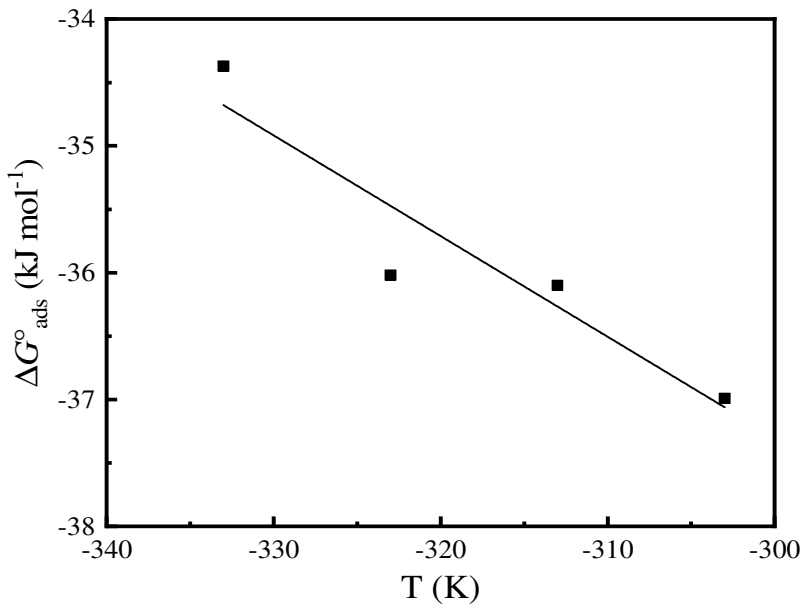

Fig. 9. Variation of ΔG^{o}_{ads} *vs* T for M-steel /1 M HCl / 5-AMT system.

The positive values of ΔS^{o}_{ads} indicate an increase in the entropy and is a consequence of the adsorption of 5-AMT on the M-steel surface [66]. Moreover, physisorption or mixture of chemi/physisorption is usually characterized by an exothermic process ($\Delta H^{o}_{ads} < 0$) [4,67]. In our case, the adsorption is exothermic accompanied by ΔS^{o}_{ads} of positive sign. It should be noted that an exothermic process of adsorption is always accompanied by increased disorder ($\Delta S^{o}_{ads} > 0$). The same phenomenon has been interpreted by several authors as desorption of water molecules existing on the metal surface and replacing them by adsorption of organic compounds [68-71].

3.5. XPS study

To more assess the adsorbed layer on the M-steel surface and to understand the corrosion protection mechanism of 5-AMT, the XPS analyses were consequently realised. The obtained XPS wide-scan (survey) spectra of pure 5-AMT and of 5-AMT/treated M-steel are presented in Fig. 10 and show the presence of C, O, N and S elements in the case of pure 5-AMT, peaks of Fe and Cl are also detected in case of 5-AMT/treated M-steel. The XPS deconvoluted profiles for different elements core levels, exploiting the CASA XPS software, are given in Figs. 11-12 and the corresponding data are recapitulated in Table 8.

For 5-AMT/treated M-steel sample, the C 1s peak deconvolution may be fitted into three components as depicted in Fig. 11 and Table 8. The first at 284.9eV is related to C–C, C=C and C–H bonds in the 5-AMT molecules [72]. The second at 286.6 eV might be attributed to C–S, C=N bonds, and C–O in methoxy group of 5-AMT [72,73]. The last at 289.1 eV and less intense component (9 %) can be associated to shake-up satellite due to π-π^* transitions in aromatic ring of 5-AMT [73]. Comparison of the component shape of C 1s peak of 5-AMT-treated M-steel (Fig. 11a) and pure 5-AMT (Fig. 12a) shows, in both cases, three

1 components approximatively at the same binding energies as described above, with slight
2 variation in the component contribution (Table 8). The presence of different carbon
3 environments on the M-steel surface clearly discloses the adsorption of 5-AMT molecules.

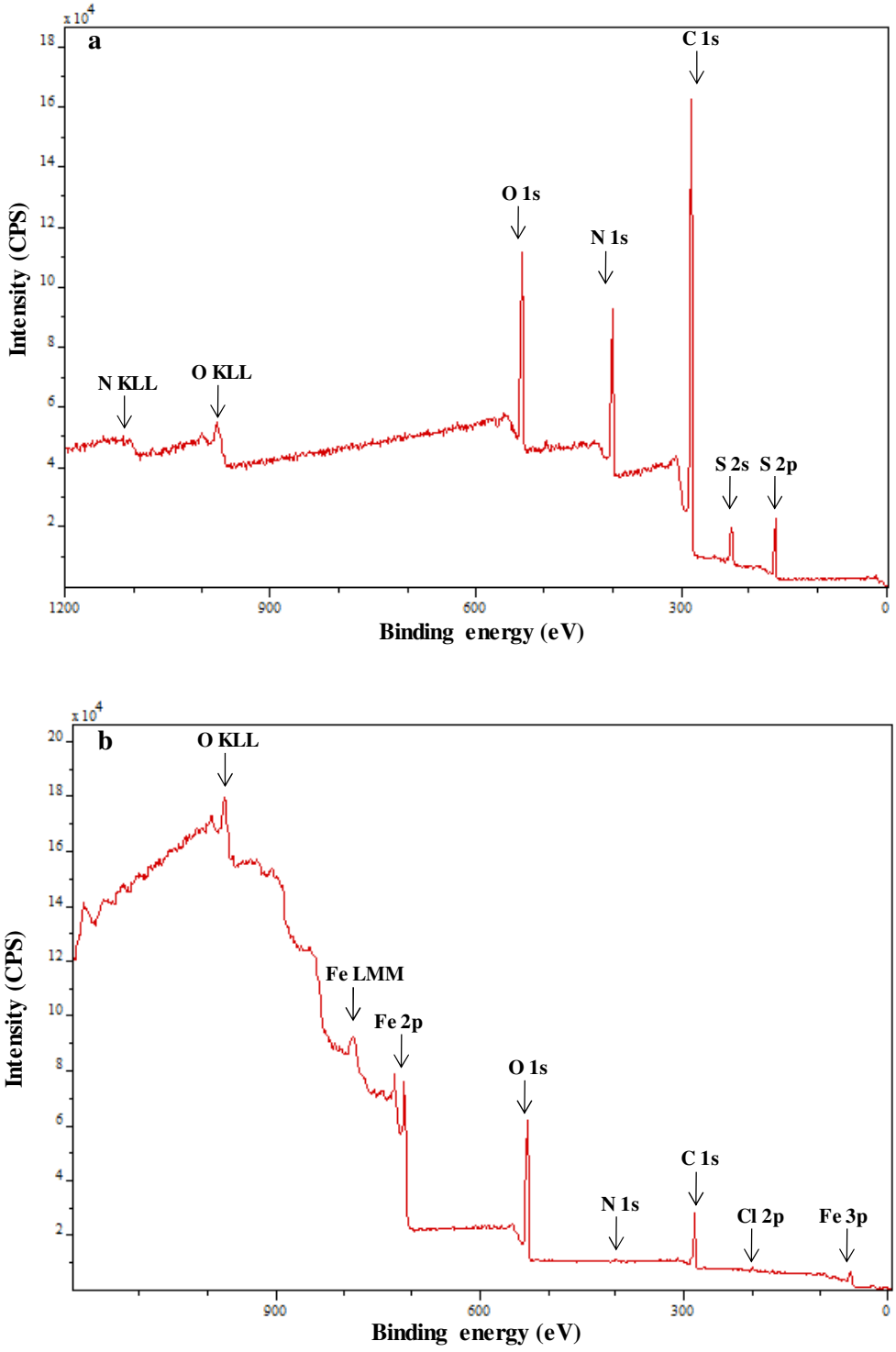

4

5

6 **Fig. 10.** XPS survey spectra of a- pure 5-AMT and b- 5-AMT/treated M-steel substrate.

7

The S 2p spectrum of the pure 5-AMT (Fig. 12d) can be resolved two spin-orbit-split doublets (S $2p_{3/2}$ and S $2p_{1/2}$), at about 162.1 and 163.2 eV, respectively. This former is ascribed to sulfur atoms in the 1,3,4-thiadiazole ring as described previously [34,74]. After immersion in 1 M HCl, no S 2p signal is detected on the surface 5-AMT treated M-steel as evidenced the XPS survey spectrum in Fig. 10b. N 1s spectrum of M-steel treated with 5-AMT in 1 M HCl shows one peak located at around 399 - 402 eV (Fig. 11b). The low intensity of this spectrum implies the low N amount on the substrate surface comparing with that of pure 5-AMT (Fig. 10b). This peak can be partly associated to =N– structure in the 1,3,4-thiadiazole ring, as confirmed in N 1s spectrum of pure 5-AMT (Fig. 12b), and partly attributed to N^+, due to protonation of nitrogen atom in the amino group ($–NH_3^+$) of 5-AMT in HCl medium [75]. However, XPS surface elemental analysis of 5-AMT treated M-steel sample shows that the N amount is very low (1.18 %). The low nitrogen content and the absence of the sulphur on the M-steel surface can provide a reasonable explanation of the 5-AMT adsorption mode. Based on this finding, we can suggest that 5-AMT inhibitor is mainly electrostatically adsorbed on the M-steel surface. Indeed, the 5-AMT molecule possesses a non-plane structure, which unfavourable for strong adsorption and therefore the N and S atoms in 5-AMT cannot be engaged actively in the surface coverage.

The O 1s spectrum for 5-AMT/treated M-steel may be deconvolutted into three components (Fig. 11c, Table 8), however, it is impossible to separate the contributions of organic and inorganic oxygen [76]. The first one at 530.1 eV could be assigned to O^{2-} in the Fe_2O_3 [68], the second at 531.7 eV can be associated to the presence of FeOOH [77] and the last one at 533.3 eV may be ascribed to O atom of adsorbed water [77]. The two higher binding energy features at 531.7 eV and 533.3 eV can be also attributed to -O- in the methoxy group of 5-AMT [78], as demonstrated by O 1s analysis of the pure 5-AMT (Fig. 12c). The presence of these components may suggest the chemical bonding between O and M-steel

surface. Indeed, the adsorption of 5-AMT via O of methoxy group can be occurred with the formation of the O-Fe bond on the basis of donor acceptor interactions between the lone sp^2 electron pairs present on the O of methoxy group and the vacant d orbitals of Fe. Moreover, the XPS surface elemental analyses show that the O concentration is higher in the case of 5-AMT/treated M-steel sample (37.85%) compared to that of pure 5-AMT (9.78 %). This difference may be explained by the formation of Fe_2O_3/FeOOH layer on the M-steel surface where 5-AMT molecules can be incorporated.

Fe 2p spectrum for substrate surface treated with 5-AMT shows a double peak profile at 711 eV (Fe $2p_{3/2}$) and 725 eV (Fe $2p_{1/2}$) as shown in Fig. 11e. The Fe $2p_{3/2}$ deconvolution consists in three components at 706.9, 710.6, and 711.3 eV (Fig. 11d, Table 8). The first one is related to Fe^0 [79], while the last two assigned to Fe (III) are associated to the presence of the Fe_2O_3 and FeOOH [80,81] as detected in the O 1s spectrum. The Cl 2p core-level is fitted on two spin–orbit-split doublets (Cl $2p_{1/2}$ and Cl $2p_{3/2}$) [75], with binding energy for Cl $2p_{3/2}$ peak at 198.5 eV (Fig. 11e) associated to Cl–Fe bond in $FeCl_3$ as mentioned previously [82]. In contrast, the XPS surface elemental analysis shows the presence of a small amount of chlorine (0.66 %) on the exposed M-steel surface and this could be attributed to the protection action of 5-AMT molecules.

In conclusion, the XPS results are in good trend with the thermodynamic findings, suggesting that the adsorption of 5-AMT on the M-steel surface involved both physisorption and chemisorption. The addition of 5-AMT in the corrosive solution leads to reduce the attack of acid ions as well as restraining the metal dissolution process simultaneously.

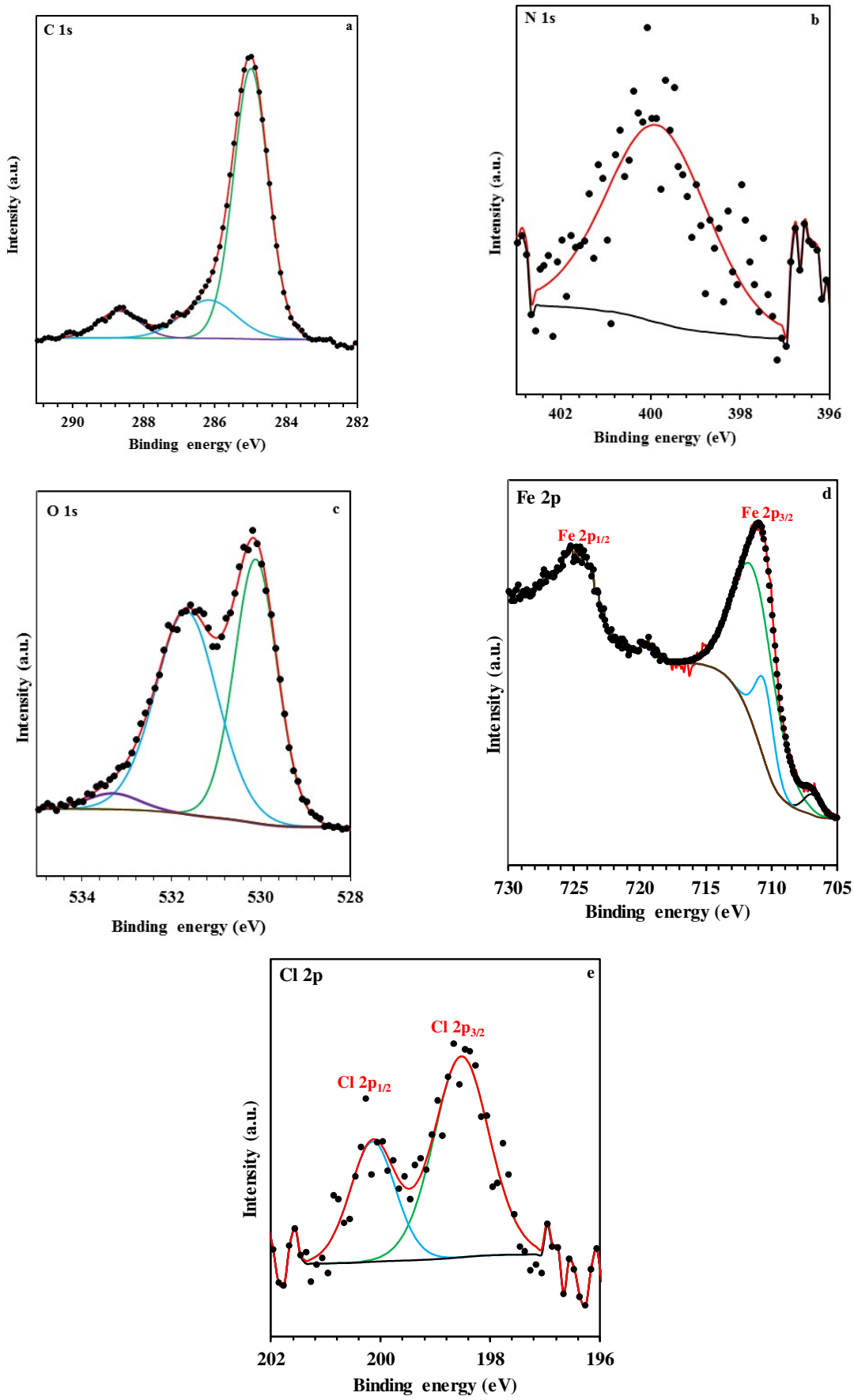

1 **Fig. 11.** XPS deconvoluted profiles of C 1s, N 1s, O 1s, Fe 2p and Cl 2p for 5-AMT/ treated M-steel.

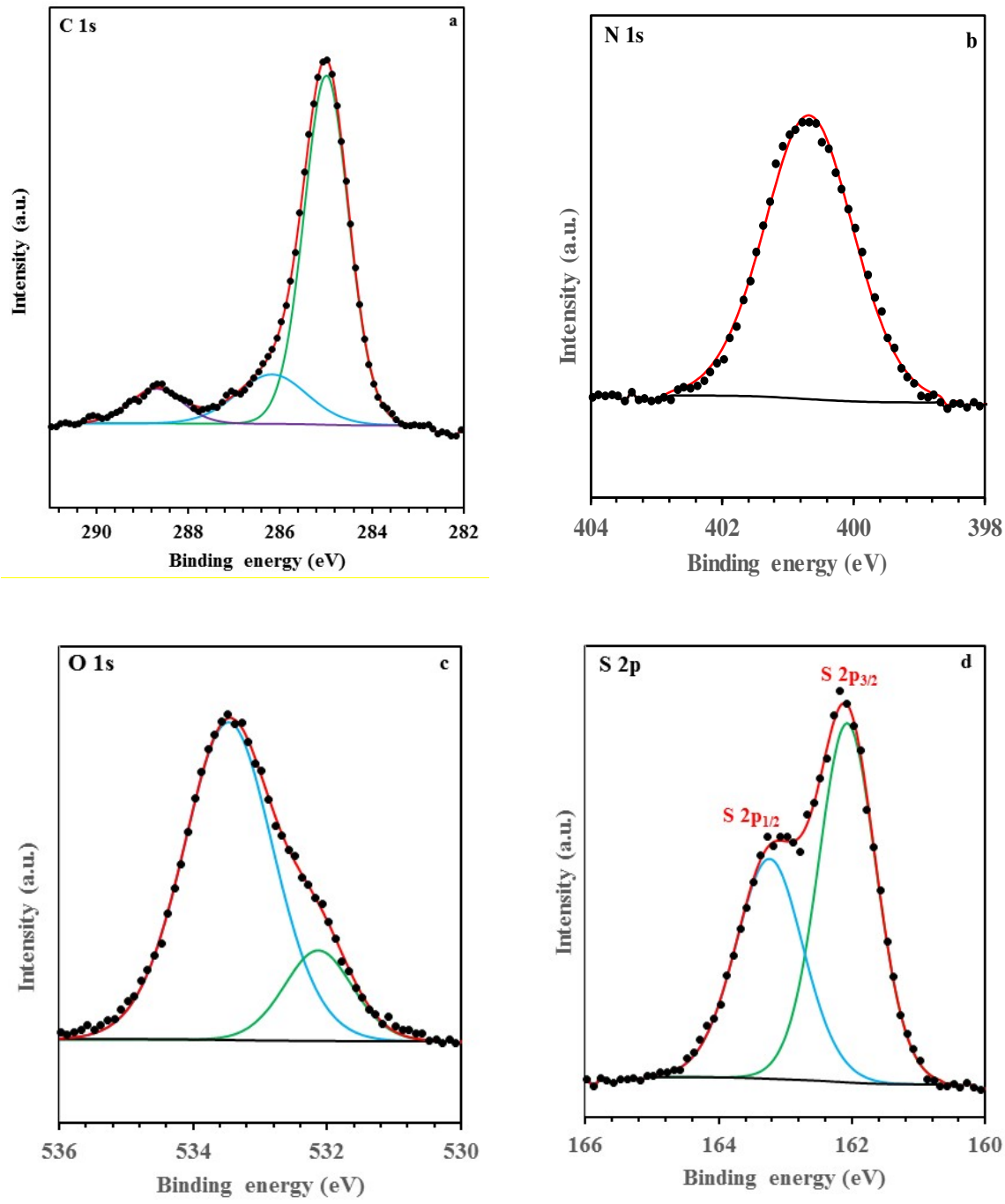

1 **Fig. 12.** XPS deconvoluted profiles of C 1s, N 1s, O 1s, and S 2p for the pure 5-AMT.

2

3

Table 8

Binding energies (eV), relative intensity and their assignment for the major core lines observed pure 5-AMT and 5-AMT/treated M-steel substrate.

Substrate	**C 1s**		**N 1s**		**S 2p**		**O 1s**		**Fe $2p_{3/2}$**	
	BE / eV	Assignment	BE / eV	Assignment	BE / eV	Assignment	BE / eV	Assignment	BE / eV	Assignment
Pure 5-AMT	284.9 (60%)	C–C/C=C/C–H	400.7 (100 %)	=N– structure / $–NH_2$	162.1 (58 %)	>S structure S $2p_{3/2}$	532.1 (18%)	C–O	—	—
	286.6 (38 %)	C–O/C–S/C=N	—	—	163.2 (42 %)	>S structure S $2p_{1/2}$	533.5 (82 %)	C–O	—	—
	289.1 (2 %)	π-π^* shakeup satellite	—	—	—	—	—	—	—	—
5-AMT/treated M-steel	285 (74%)	C–C/C=C/C–H	398 - 402	=N– structure / $–NH_3^+$	—	—	530.1 (46 %)	O^{2-} in Fe_2O_3	706.9 (4 %)	Fe^0
	286.2 (17 %)	C–O/C–S/C=N	—	—	—	—	531.7 (51 %)	OH^- in FeOOH/ C–O	710.6 (18 %)	Fe_2O_3/FeOOH
	288.7 (9 %)	π-π^* shakeup satellite	—	—	—	—	533.3 (3 %)	H_2O_{ads}	711.3 (78 %)	FeOOH/FeCl

3.6. DFT calculations

In order to study the correlation between the inhibitor molecular structure and its anticorrosion activity, the inhibitive performances of 2-amino-5-(2-methoxyphenyl)-1,3,4-thiadiazole (5-AMT) were compared with those of 2-amino-5-thiol-1,3,4-thiadiazole (5-ATT) previously described [10]. 5-ATT is a 1,3,4-thiazole derivative, similar to 5-AMT with thiol group in 5-ATT instead of methoxyphenyl group in 5-AMT (Table 9).

Table 9
Comparison of η(%) values for 5-AMT and 5-ATT (5×10^{-4} M) in 1 M HCl at 303 K obtained by different corrosion evaluation methods.

Inhibitor	Inhibition efficiency (%)			
	Tafel	*LPR*	*AC impedance*	*Weight loss*
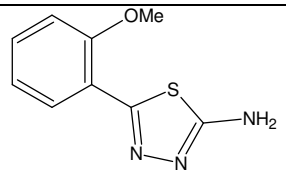 5-AMT	98.68	98.27	98.30	98.00
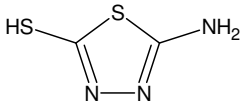 5-ATT [10]	82.50	76.96	77.71	79.48

The obtained corrosion efficiency values, obtained by different evaluation methods (Tafel polarisation, AC impedance and weight loss), for M-steel in 1 M HCl containing 5×10^{-4} M of a 1,3,4-thiazole derivative (5-AMT or 5-ATT) are listed in Table 9. The inspection of these results showed that 5-AMT presents the better inhibition performance than 5-ATT whatever the used evaluation method, which can be correlated to the difference between the two inhibitor structures. Indeed, the replacement of SH group in position 5 in 5-ATT molecule by the methoxyphenyl group in 5-AMT molecule arises a significate enhancement in the inhibition efficiency. This enhanced efficiency may be due to the introduction of the electron releasing on the 1,3,4-thiadiazole moiety, giving therefore, a favourable electron density for preferential adsorption interactions. Hence it facilitates greater adsorption of 5-AMT on M-steel surface than 5-ATT, leading to higher inhibition efficiency of 5-AMT than

5-ATT. This difference in inhibition efficiency could be explained by computational parameters of these two molecules in both neutral and protonated forms using DFT method.

3.6.1. Neutral forms of 5-ATT and 5-AMT

The electron density distribution of frontier molecular orbitals (FMOs), such as HOMO and LUMO, is very important for predicting the mode of reactivity of inhibitor molecules with the substrate surface [82]. This behaviour translates into the phenomenon of electron sharing whose donor effect is represented by the regions occupied by the electron density of HOMO, while the regions occupied by the electron density of LUMO will be available to receive electrons [83]. In this context, Fig. 13 shows the optimized structures and electron density distributions of FMOs. We note that the chemical quantum calculations show no imaginary frequency, i.e. these molecules are well optimized and stable. The visual scan of the Fig. 13 clearly indicates that the density distribution of FMOs is localized over the entire structure of the molecules in question. This shows that both compounds carry several active sites that are available to react with the iron atoms on the metal surface, indicating better adsorption and supporting the protection of the metal surface against corrosion [84].

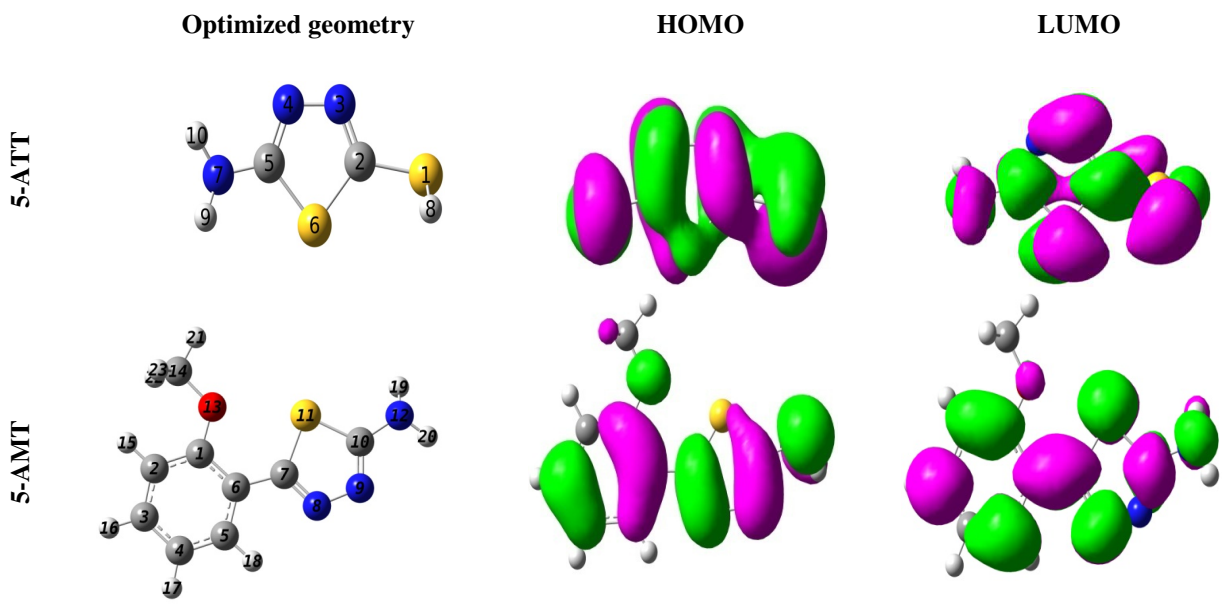

Fig. 13. Optimized structures, HOMO and LUMO for the neutral forms of 5-ATT and 5-AMT at B3LYP/6-31G (d, p) in gas phase.

The set of chemical quantum descriptors obtained by the DFT calculation of the two neutral molecules in the gas phase are grouped together in Table 10. Analysis and comparative study of the molecular descriptor values show that there is a good correlation with the order of inhibitory efficiency, i.e. 5-AMT > 5-ATT. The 5-AMT molecule has higher values of E_{HOMO} and ΔN_{110}, reflecting a strong tendency to give electrons to the vocal orbitals of iron atoms to form coordination bonds, while the electron acceptor provider is measured by the lowest value of E_{LUMO} [85,86]. The gap energy (ΔE_{gap}) is the energy required to remove an electron from the last occupied layer and reflects the degree of chemical reactivity of a molecule with a minimum value of this descriptor [87]. Therefore, compared with 5-ATT, the minimum value of ΔE_{gap} for 5-AMT indicates that this molecule has high chemical activity. Hardness (η) is another descriptor that represents the reactivity of a molecule, a minimum value of this descriptor indicates high reactivity [88]. In this case, the inhibition efficiency values of 5-AMT and 5-ATT regrouped in Table 9 are in accordance with the forecasted trend of protection efficiency. Electronegativity (χ) is exploited to examine the ability of a molecule to attract electrons to it; a molecule with a minimum descriptor value is considered a good inhibitor [89]. For 5-AMT molecule, this property can be verified. Electrophilic (ω) and nucleophilic (ε) indicators present the capacity of an inhibitory molecule to receive and contribute electrons, respectively [90]. The data in Table 10 show that a 5-AMT molecule represents a high capacity to give electrons and a low capacity to accept electrons. This characteristic indicates that 5-AMT reacts more efficiently with the metal surface by forming covalent bonds.

Table 10

Quantum chemical descriptors for the neutral forms of 5-ATT and 5-AMT at B3LYP/6-31G (d, p) in gas phase.

Neutral form	E_{HOMO} (eV)	E_{LUMO} (eV)	ΔE_{gap} (eV)	η (eV)	χ (eV)	ΔN_{110}	ω (eV)	ε (eV^{-1})
5-ATT	-6.670	-1.353	5.317	2.658	4.011	0.152	3.027	0.330
5-AMT	-5.570	-1.107	4.463	2.2315	3.338	0.332	2.497	0.400

[(a)] The η(%) values were obtained by exploiting EIS method for 5×10^{-4} M of investigated 1,3,4-thidiazole derivatives.

3.6.2. Possible protonated forms of 5-ATT and 5-AMT

As observed in the structure of the molecules studied, there are hetero atoms such as sulfur (S), nitrogen (N), and oxygen (O). It is probable that these atoms suggest their strong tendency to protonate in an acidic medium. Therefore, it is crucial to explore the importance of the molecular properties of the protonated form of the inhibitor molecule for adsorption on metal surfaces [91]. We have exploited data of distribution of protonated forms versus pH exploiting the Marvin Sketch software to determine the most favourable site(s) for protonation [92]. Therefore, Fig. 14 represents the different possible proton forms determined by nitrogen atoms for the two molecules tested. The percentage of protonation at pH = 0 of each atom is depicted in Fig. 14. It is clear that the 5-ATT molecule has only one form of the protonation 5-ATTH$^+$ (100%). On the other hand, the 5-AMT molecule has three possible protonated forms such as 5-AMTH$^+$ (form 1: 39%), 5-AMTH$^+$ (form 2: 37%), and 5-AMTH$_2^{2+}$ (form 3: 24%). The percentage of the only protonation for the two nitrogen atoms is almost the same, while the percentage of double protonation is less important than single protonation. This diversity of protonated sites indicates a high level of reactivation of the 5-AMT molecule in the acidic medium. This explains why this molecule is more effective against corrosion than 5-AMT. In the following, we investigated the effect of protonation on the electronic behaviour of the molecules surveyed exploiting DFT calculation.

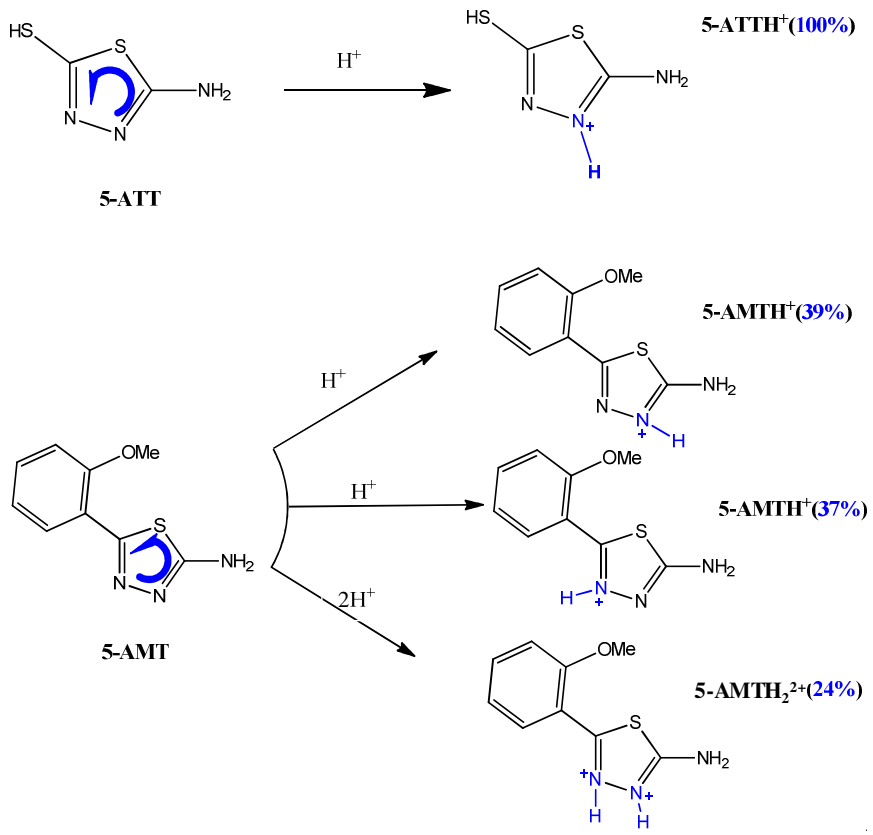

Fig. 14. Possible forms of protonation of 5-ATT and 5-AMT in the acidic medium.

The optimized structures and electron density distribution of FMOs in the ground state of the protonated forms of the 5-ATT and 5-AMT molecules are displayed in Fig. 15. It is clear from analysis of this figure that the density of HOMO and LUMO is dispersed over the entire molecular skeleton of all protonated forms, i.e. all the atoms of the molecules studied are capable of reacting with the iron atoms of the metal surface. This result proves that the protonation of the selected molecules does not influence the electron density distribution, which leads to a better adsorption of these forms on the surface of the substrate. The different values of quantum chemical descriptors calculated of the selected molecules in the protonated form exploiting at B3LYP/6-31G (d, p) are shown in Table 11. Comparative analysis of the results accumulated in this Table suggests that all protonated forms of 5-AMT are more chemically reactive than the protonated form of 5-ATT. This also confirms the order of inhibitory efficacy observed experimentally.

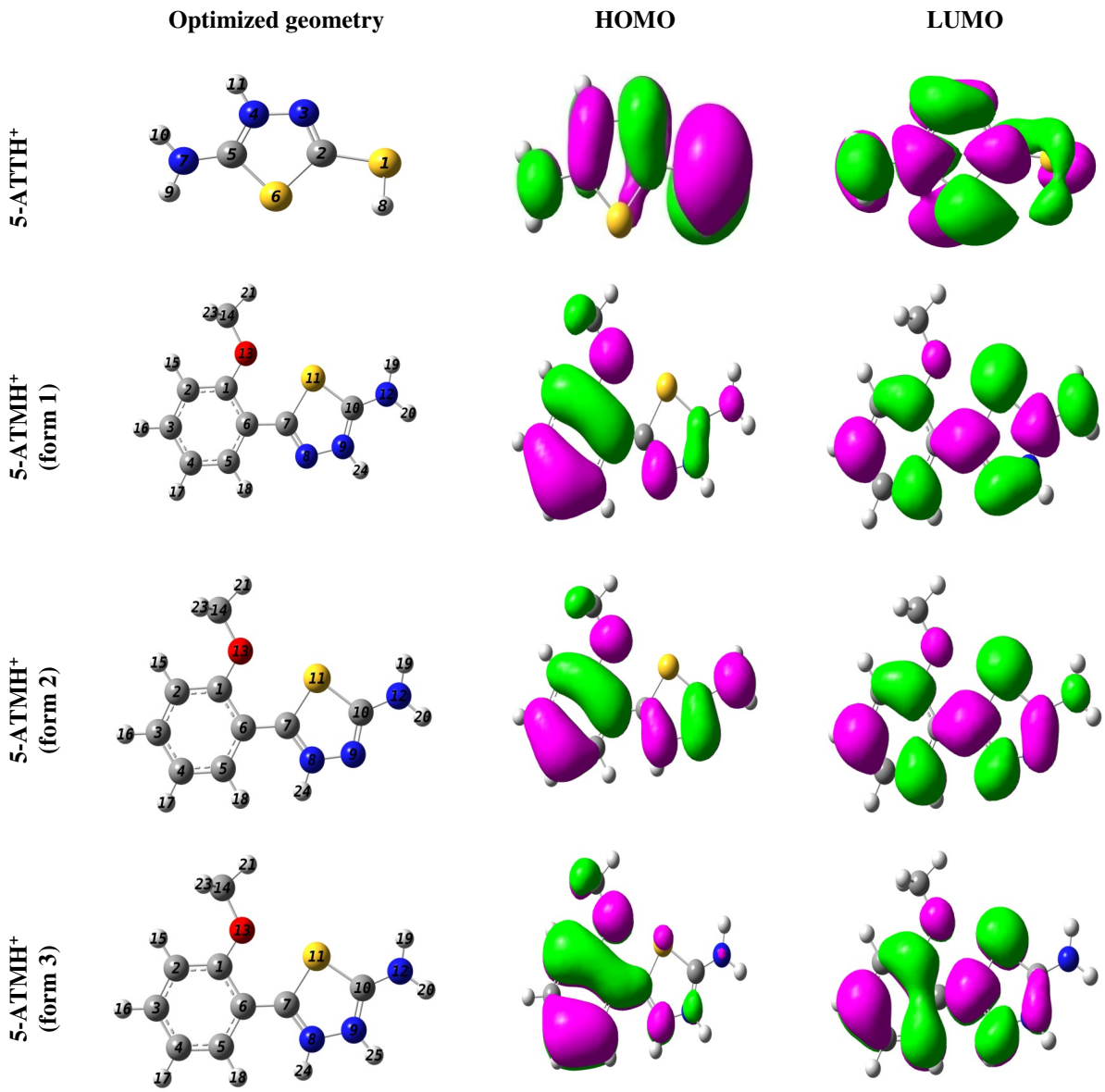

Fig. 15. Optimized structures, HOMO and LUMO for the protonated forms of 5-ATT and 5-AMT at B3LYP/6-31G (d, p) in gas phase.

Generally speaking, protonation results in an increase in the reactivated of protonated molecules, this is justified by a decrease in the values of the descriptors ΔE_{gap} and η. In addition, the high values of E_{LUMO}, ω and χ, as well as the negative values of ΔN_{110}, of the protonated forms are characterized by a high electron receptor effect from the electron donor group located in the metal surface [93]. This effect is very important in the case of double protonation (5-AMTH$_2^{2+}$ (24%)).

Table 11
Quantum chemical descriptors for the protonated forms of 5-ATT and 5-AMT at B3LYP/6-31G (d, p) in gas phase.

Possible protonated forms	E_{HOMO} (eV)	E_{LUMO} (eV)	ΔEgap (eV)	η (eV)	χ (eV)	ΔN_{110}	ω (eV)	ε (eV^{-1})
5-ATTH^+	-11.229	-6.178	5.051	2.525	8.703	-0.769	14.997	0.067
5-AMTH^+ (form 1)	-9.466	-5.267	4.199	2.099	7.366	-0.606	12.923	0.077
5-AMTH^+ (form 2)	-9.864	-5.979	3.885	1.942	7.921	-0.798	16.152	0.062
5-AMTH_2^{2+} (form 3)	-13.639	-10.158	3.481	1.740	11.898	-2.033	40.671	0.025

3.6.3. Local selectivity (Fukui indices)

In order to identify the local selectivity of the inhibitory molecules 5-ATT and 5-AMT, the Fukui functions were calculated exploiting the DMol[3] module integrated in the Materials Studio package (version 8.0) [94]. In this analysis, the Generalized Gradient Approximation (GGA) of the Perdew-Burke-Ernzerhof (PBE) formula was employed for the electron exchange potential-electron correlation [95], and the all-electron computations were carried out with a double numerical basis (DNP 4.4). Fukui functions allow describing the reactive sites that are responsible on the electrophilic (f_i^-) and nucleophilic (f_i^+) attacks of the molecules under review. Generally, the most condensed functions show the most active sites (atoms) [96]. Fig. 16 illustrates the densities of the Fukui functions for neutral and protonated molecules for electrophilic (cyan color) and nucleophilic (wine color) attacks. The general observation that is noted from this figure, the protonation leads to decreased density of f_i^- (cyan color), i.e. the donor power of electrons is reduced by this effect. In addition, the majority of sites in the structure of neutral molecules are occupied by condensed functions (f_i^- and f_i^+), indicating high reactivity with sites on the metal surface.

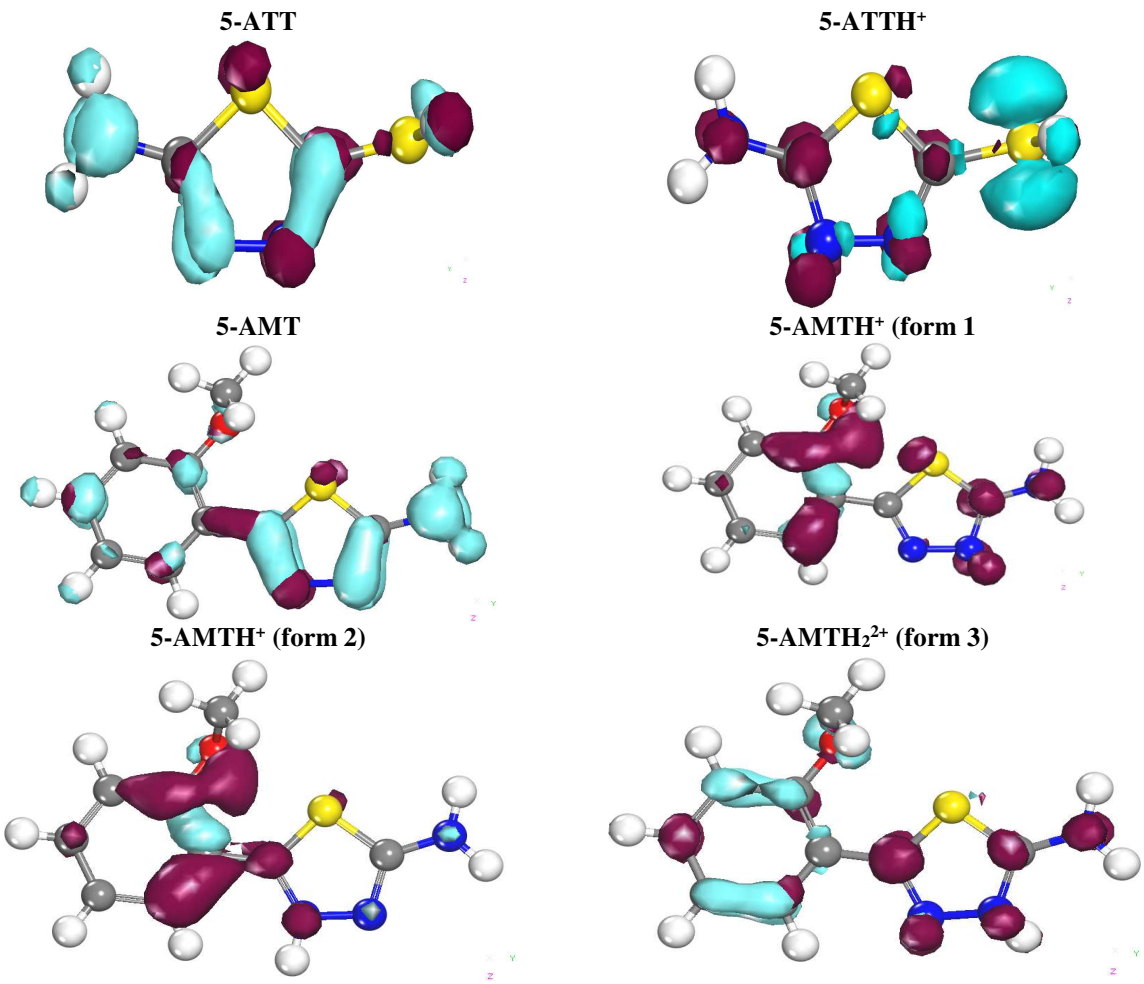

Fig.16. Condensed Fukui functions (f_i^- (cyan color) and f_i^+ (wine color)) distributed on the skeleton of neutral and protonated inhibitory molecules.

3.7. MDS evaluation

3.7.1. Neutral form/Fe (110) interface

The protection of a metal surface by inhibitor molecules depends on the mechanism of action, i.e. the adsorption performance [97]. Therefore, to obtain more information on this phenomenon, molecular dynamics simulation (MDS) was exploited, taking into account the considerations of the corrosive medium (HCl) [98,99]. Fig. 17 gives the best adsorption configuration of the neutral molecules of 5-ATT and 5-AMT on the Fe (110) surface.

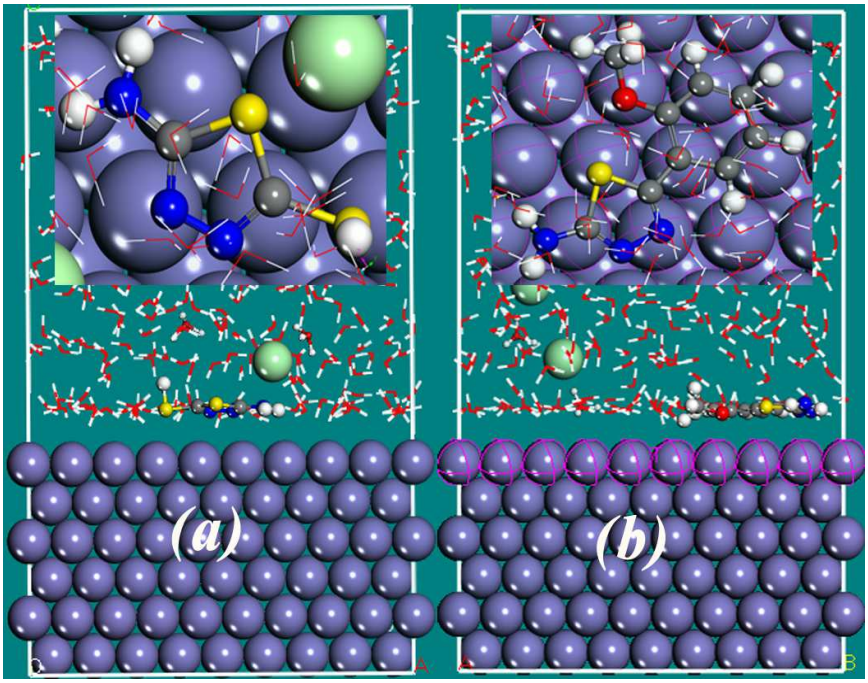

Fig. 17. Constant adsorption configurations of (a) 5-ATT and (b) 5-AMT neutral molecules on the Fe (110) surface in HCl at 303 K.

It was very apparent that the tested molecules are adsorbed by the whole molecular structure, covering a large part of the contact surface. The advantage of the 5-AMT molecule is a large molecular surface area skeleton caused by the presence of methoxyphenyl group compared of 5-ATT, resulting in the best protection of the M-steel surface. In addition, parallel adsorption indicates that 5-ATT and 5-AMT compounds exhibit several local active sites, revealing high chemical reactivity of these species.

The energy descriptors, i.e. the interaction energy ($E_{\text{interaction}}$) and the binding energy (E_{binding}), are exploited to evaluate the interaction and adsorption power of the tested inhibitory molecules with the Fe (110) surface, respectively. To calculate the values of the two energy descriptors mentioned, we exploited the two following equations [100]:

$$E_{\text{interaction}} = E_{\text{total}} - (E_{\text{surface+solution}} + E_{inhibitor}) \quad \text{(Eq. 12)}$$

$$E_{\text{binding}} = -E_{\text{interaction}} \quad \text{(Eq. 13)}$$

The calculated values of $E_{interaction}$ and $E_{binding}$ of the adsorbed molecules are collected in Table 12. As noted in this table, the negative values of $E_{interaction}$ and the positive and high values of $E_{binding}$ indicate that the adsorption process of the molecules under discussion occurs spontaneously and that 5-ATT and 5-AMT adsorb efficiently on the substrate surface [101]. Therefore, compared with 5-ATT, the high value of $E_{binding}$ of 5-AMT shows that this molecule is more effective against M-steel corrosion in acidic medium [102]. This result reinforces the order of inhibitory efficacy reported in Table 9.

Table 12
$E_{interaction}$ and $E_{binding}$ energies for 5-ATT and 5-AMT on the Fe (110) surface at 303 K.

System	$E_{interaction}$ (kJ mol^{-1})	$E_{binding}$ (kJ mol^{-1})
5-ATT / Fe(110)	-342.239	342.239
5-AMT / Fe(110)	-389.820	389.820

3.7.2. Protonated form/Fe (110) interface

In the DFT section, we have already discussed that protonation leads to an increase in the overall chemical reactivity of the protonated forms. A similar study was conducted exploiting MDS. Fig. 18 shows the different final adsorption configurations of different protonated forms of the molecules in question. The visual inspection of the images portrayed in the side and top views shows that despite protonation the molecules are still adsorbed by the entire molecular structure. This reflects a better reactivated of the investigated compounds with the metallic surface, indicating a better protection of the examined M-steel.

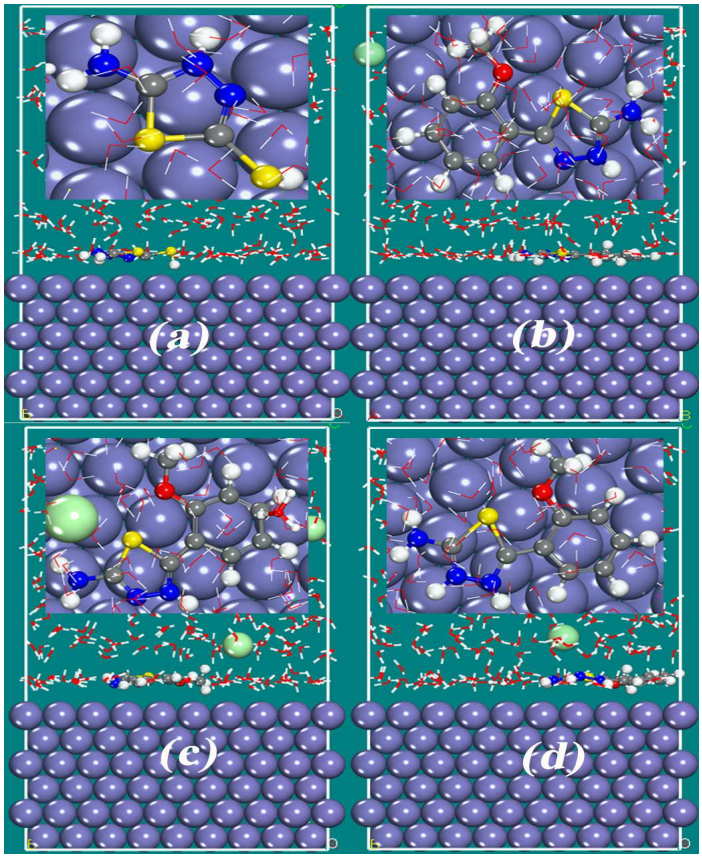

Fig. 18. Constant adsorption configurations of (a) 5-ATTH$^+$ (100%), (b) 5-AMTH$^+$ (form 1), (c) 5-AMTH$^+$ (form 2), and (d) 5-AMTH$_2^{2+}$ (form 3) protonated molecules on the Fe (110) surface in 1 M HCl at 303 K.

To better understand the effect of protonation on the reactivity of the studied molecules with the metal surface, we exploited energy descriptors such as $E_{\text{interaction}}$ and E_{binding}. The values of these descriptors are grouped in Table 13. It is very clear that the of $E_{\text{interaction}}$ are shifted towards the most negative of all protonated forms, leading to an increase in the reactivity of the forms in relation to the surface of the contact, *i.e.* the protonation positively influences the inhibitor/Fe interfacial interaction. In addition, the more positive values of the protonated forms in comparison with the neutral forms indicate that these forms are well adsorbed on the surface of the iron. There is also increased reactivity in the case of double protonation of 5-AMT. Similarly, protonation does not change the order of effectiveness discovered experimentally.

Table 13
$E_{interaction}$ and $E_{binding}$ energies for 5-ATTH$^+$, 5-AMTH$^+$ (form 1), 5-AMTH$^+$ (form 2), and 5-AMTH$_2^{2+}$ (form 3) protonated molecules on the Fe (110) surface at 303 K.

System	$E_{interaction}$ (kJ mol^{-1})	$E_{binding}$ (kJ mol^{-1})
5-ATTH$^+$ / Fe(110)	-365.015	365.015
5-AMTH$^+$ (form 1) / Fe(110)	-406.981	406.981
5-AMTH$^+$ (form 2) / Fe(110)	-4013.204	4013.204
5-AMTHH^{2+} (form 3) / Fe(110)	-429.979	429.979

3.8.2. RDF method

The adsorption of inhibitor molecules on the surface of the metal depends essentially on the types of bonds formed between them [103]. The radial distribution function (RDF) method emphasizes the structural analysis of the MD simulation results and has been employed to detect the type of chemical, physical, or both chemical and physical bonds. If the value of these lengths is of the range of 1-3.5 Å, in this case there is the appearance of the chemical aspect, indicating a strong adsorption, while if the bond length value is > 3.5 Å, then the physical appearance occurs easily [104]. Figs. 19 and 20 reveal that the observed values on the first peak for each bond length of the adsorption of neutral and protonated molecules on the surface of Fe (110) at the simulated temperature of 303 K are in the chemisorption range for the bond lengths depicted in these figures. These results show that both forms adsorb on the metal surface through coordination bonds.

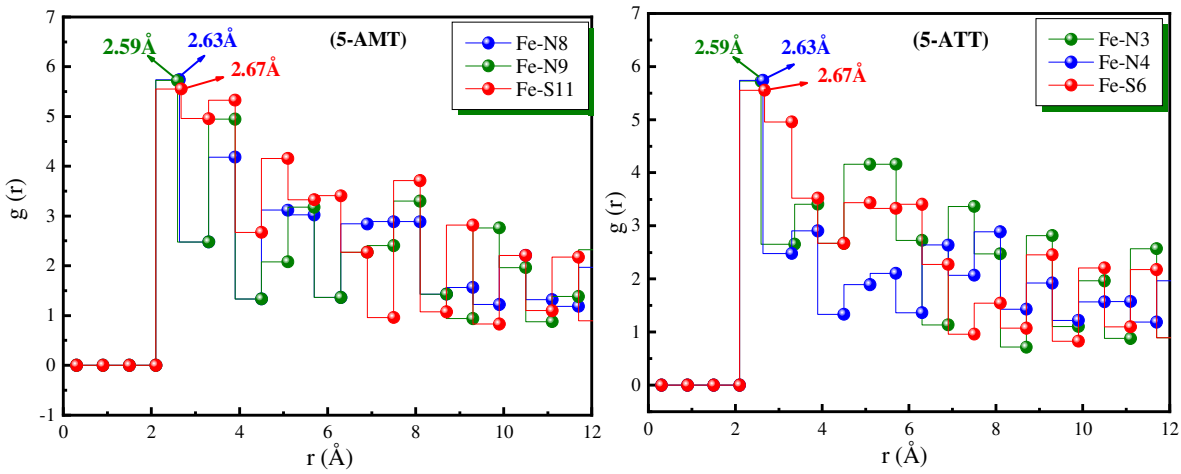

Fig. 19. RDF method of neutral forms on Fe (110) surface in HCl solution at 303 K obtained exploiting MD simulation.

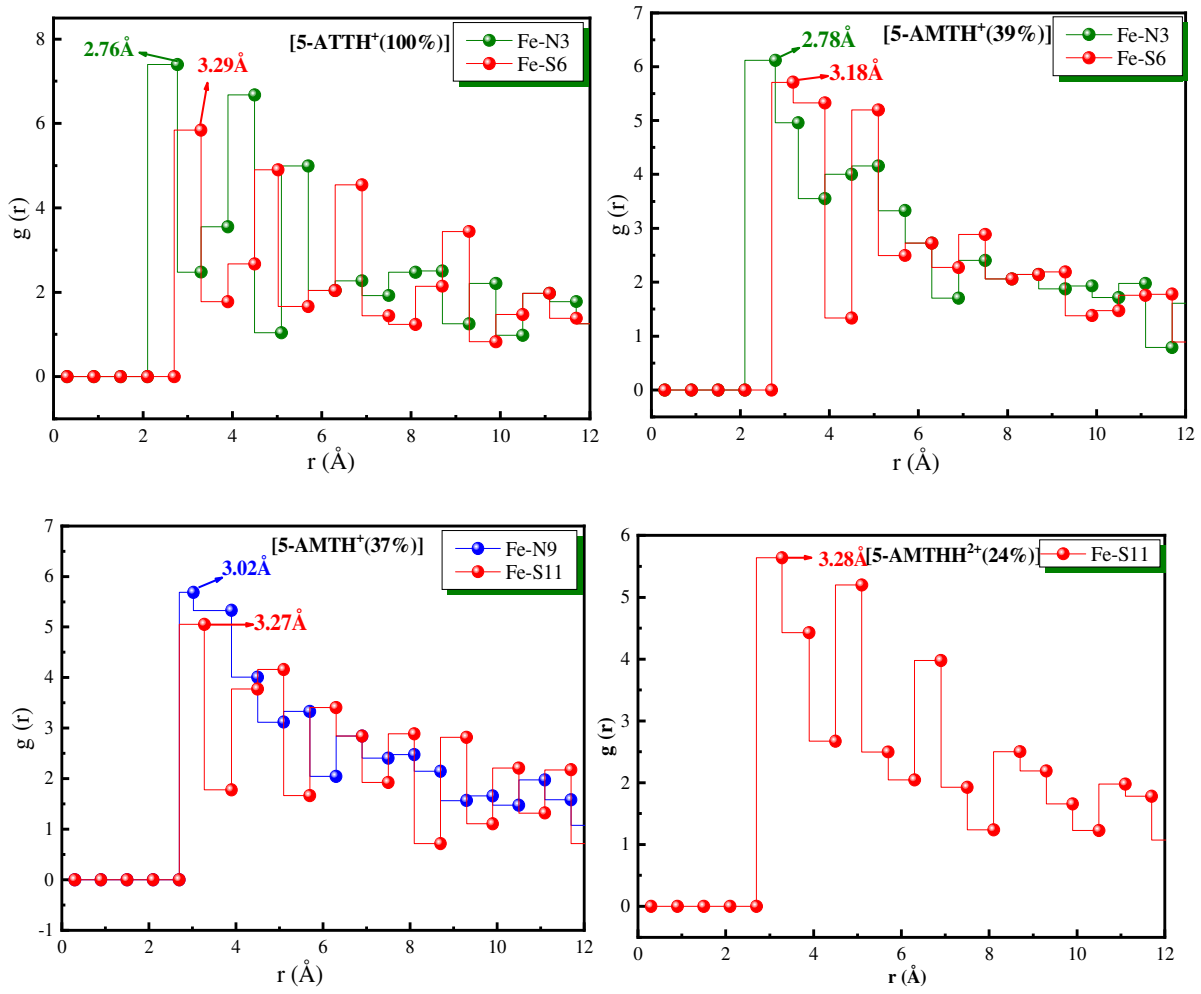

Fig. 20. RDF method of protonated forms of 5-ATT and 5-AMT on Fe (110) surface in 1 M HCl solution at 303 K obtained exploiting MD simulation.

4. Conclusions

2-Amino-5-(2-methoxyphenyl)-1,3,4-thiadiazole (5-AMT) was found to show excellent protection properties for M-steel corrosion in 1 M HCl solution and the maximum protection efficiency is about 98% at 5×10^{-4} M at 303 K. PDP technique indicates that the tested 1,3,4-thiadiazole is a mixed type corrosion inhibitor in 1 M HCl medium. EIS measurements show that the polarisation resistance (R_p) increased and the double layer capacitance (C_{dl}) decreased in the presence of 5-AMT indicating the adsorption of this inhibitor on the M-steel surface. The adsorption of 5-AMT obeyed to Langmuir adsorption isotherm and the thermodynamic results as well as XPS study further suggested the combination of physisorption and chemisorption. Both the computational DFT calculations and MD simulation outcomes showed the reasonable correlations between the anti-corrosion activity of the tested inhibitor and their chemical structure properties.

References

[1] V.S. Sastri, Corrosion Inhibitors-Principles & Applications, Wiley, Chichester, England, 1998.
[2] R. Solmaz, G. Kardas, B. Yazıcı, M. Erbil, Corros. Eng. Sci. Technol. 43 (2008) 186–191.
[3] S.A. Abd El Maksoud, Corros. Sci. 44 (2002) 803–813.
[4] A.Y. Musa, A.A.H. Kadhum, A.B. Mohamad, M.S. Takriff, Corros. Sci. 52 (2010) 3331–3340.
[5] I. Ahamad, R. Prasad, M.A. Quraishi, Corros. Sci.52 (2010) 3033–3041.
[6] H. Ma, S. Chen, L. Niu, S. Zhao, S. Li, D. Li, J. Appl. Electrochem. 32 (2002) 65–72.
[7] F. Bentiss, M. Outirite, M. Traisnel, H. Vezin, M. Lagrenée, B. Hammouti, S.S. Al-Deyab, C. Jama, Int. J. Electrochem. Sci. 7 (2012) 1699–1723.
[8] T.A. Salman, D.S. Zinad, S.H. Jaber, M. Al-Ghezi, A. Mahal, M. Takriff, A.A. Al-Amiery, J. Bio. Tribo. Corros. 5, Article number 48 (2019).
[9] S.B. Al-Baghdadi, F.G. Hashim, A.Q. Salam, T.K. Abed, T.S. Gaaz, A.A. Al-Amiery, A.A.H. Kadhum, K.S. Reda, W.K. Ahmed, Results Phys. 8 (2018) 1178–1184.
[10] H. Ouici, M. Tourabi, O. Benali, C. Selles, C. Jama, A. Zarrouk, F. Bentiss, J. Electroanal. Chem. 803 (2017) 125–134.
[12] S.B. Al-Baghdadi, F.T.M. Noori, W.K. Ahmed, A.A. Al-Amiery, J. Advan. Electrochem. 2(1) (2016) 67–69.
[13] M.J. Banera, J.A. Caram, C.A. Gervasi, M.V.Mirífico, J. Appl. Electrochem. 44 (12) (2014) 1337–1344.
[14] A.A. Al-Amiery, A.A. H. Kadhum, A.H.M. Alobaidy, A. B. Mohamad, P.S. Hoon, Materials 7 (2014) 662–672.
[15] M. Sobhi, R. El-Sayed, M. Abdallah, J. Surf. Deterg. 16 (2013) 937–946.
[16] M. Palomar-Pardavé, M. Romero-Romo, H. Herrera-Hernández, M.A. Abreu-Quijano, N.V. Likhanova, J. Uruchurtu, J.M. Juárez-García, Corros. Sc. 54 (2012) 231–243.
[17] F. Bentiss, B. Mernari, M. Traisnel, H. Vezin, M. Lagrenée, Corros. Sci. 53 (2011) 487–495.
[18] R. Solmaz, Corros. Sci. 52 (2010) 3321–3330.
[19] A.K. Singh, M.A. Quraishi, Corros. Sci. 52(2010) 1373–1385.
[20] Y. Tang, X. Yang, W. Yang, Y. Chen, R. Wan, Corros. Sci. 52 (2010) 242–249.
[21] R. Solmaz, G. Kardaş, B. Yazici, M. Erbil, Coll. Surf. A: Physicochem. Eng. Aspects 312 (2008) 7–17.
[22] F. Bentiss, M. Lebrini, M. Lagrenée, M. Traisnel, A. Elfarouk, H.Vezin, Electrochim. Acta 52 (2007) 6865–6872.
[23] R.T. Loto, C.A. Loto, Protec. Met. Phys. Chem. Surf. 51 (2015) 693–700.
[24] R.T. Loto, C.A. Loto, A.P.I. Popoola, T.I. Fedotova, Portugaliae Electrochim. Acta 32 (2014) 337–354.
[25] M. Guzmán, R. Lara, L. Vera, J. Chill. Chem. Soc. 54(2009) 123–128.
[26] A. Benikdes, O. Benali, A. Tidjani, M. Tourabi, H. B. Ouici, F. Bentiss, J. Mater. Environm.Sci. 8(2017) 3175–3183.
[27] W. Qafsaoui, A. Et Taouil, M.W. Kendig, O. Heintz, H. Cachet, S. Joiret, H. Takenouti, J. Appl. Electrochem. 49 (2019) 823–837.
[28] M.B. Radovanović, M.M. Antonijević, J. Adhes. Sci. Tech. 31 (2017) 369–387.
[29] H. Tian, W. Li, K. Cao, B. Hou, Corros. Sci. 73 (2013) 281–291.
[30] O.L. Blajiev, T. Breugelmans, R. Pintelon, H. Terryn, A. Hubin, Electrochim. Acta, 53(2008) 7451–7459.
[31] E.M. Sherif, S. Park, Electrochim. Acta 51 (2006) 6556–6562.
[32] O. Blajiev, A. Hubin, Electrochim. Acta 49 (2004) 2761–2770.
[33] M. Yusuf, R.A. Khan, B. Ahmed, Bioorg. Med. Chem. 16 (2008) 8029–8034.
[34] M. Tourabi, K. Nohair, M. Traisnel, C. Jama, F. Bentiss, Corros. Sci. 75 (2013) 123–133.
[35] D.A. Shirley, Phys. Rev. B 5 (1972) 4709–4714.
[36] F. Benhiba, H. Zarrok, A. Elmidaoui, M. El Hezzat, R. Touir, A. Guenbour, A. Zarrouk, S. Boukhris, H. Oudda, J. Mater. Environ. Sci. 6 (2015) 2301–2314.
[37] B. Tana, S. Zhang, H. Liu, Y. Qiang, W. Li, L. Guo d, S. Chen, J. Taiwan. Inst. Chem. E. 102 (2019) 424–437.

[38] M. Frisch, G. Trucks, H.B. Schlegel, G. Scuseria, M. Robb, J. Cheeseman, G. Scalmani, V. Barone, B. Mennucci, G. Petersson, Gaussian 09, revision D. 01, Gaussian, Inc., Wallingford CT, 2009.
[39] L. Saqalli, M. Galai, F. Benhiba, N. Gharda, N. Habbadi, R. Ghailane, M. Ebn Touhami, Y. Peres-lucchese, A. Souizi, R. Touir, J. Mater. Environ. Sci. 8 (2017) 2455–2467.
[40] F. Benhiba, H. Serrar, R. Hsissou, A. Guenbour, A. Bellaouchou, M. Tabyaoui, S. Boukhris, H. Oudda, I. Warad, A. Zarrouk, Chem. Phys. Lett. 743 (2020) 137181
[41] S. Kaya, P. Banerjee, S.K. Saha, B. Tüzün, C. Kaya, RSC Adv., 6 (2016) 74550–74559.
[42] Materials Studio, Revision 8.0, Accelrys Inc., San Diego, USA (2015).
[43] H. Sun, J. Phys. Chem. B. 102 (1998) 7338–7364.
[44] H.C. Andersen, J. Chem. Phys. 72 (1980) 2384–2393.
[45] C. Verma, J. Haque, E.E. Ebenso, M.A. Quraishi, Results Phys. 9 (2018) 100–112
[46] A. Singh, K. R. Ansari, M.A. Quraishi, H. Lgaz, Materials 12 (2019) 17–35.
[47] I. Nadi, Z. Belattmania, B. Sabour, A. Reani, A. Sahibed-dine, C. Jama, F. Bentiss, Int. J. Biol. Macromol. 141 (2019) 137−149.
[48] A. Espinoza-Vázquez, S. Garcia-Galan, F. J. Rodríguez-Gómez, J. Anal. Bioanal. Tech. 6 (2015) 1000273.
[49] A.S. Fouda, K. Shalabi, R. Ezzat, J. Mater. Environ. Sci. 6 (2015) 1022–1039.
[50] M. Lebrini, M. Lagrenée, H. Vezin, M. Traisnel, F. Bentiss, Corros. Sci. 49 (2007) 2254–2269.
[51] F. Bentiss, M. Traisnel, M. Lagrenée, J. Appl. Electrochem. 31 (2001) 41–48.
[52] R. Yildiz, Corros. Sci. 90 (2015) 544–553.
[53] M. Yadav, U. Sharma, P.N. Yadav, Egyp. J. Petrol. 22 (2013) 335–344.
[54] I.N. Putolova, S.A. Balezin, V.P. Barannik, Metallic Corrosion Inhibitors, Pergamann Press, NY, 1960, 31.
[55] R. Solmaz, G. Kardaş, M. Çulha, B. Yazıcı, M. Erbil, Electrochim. Acta 53 (2008) 5941−5953.
[56] M. Scendo, J. Trela, Inter. J. Electrochem. Sci. 8(2013) 8329–8347.
[57] Q.A. Jawad, D.S. Zinad, R.D. Salim, A.A. Al-Amiery, T.S. Gaaz, M.S. Takriff, A.A.H. Kadhum, Coatings 9 (2019) 729.
[58] A.K. Singh, J. Appl. Electrochem. 40 (2010) 1293–1306.
[59] G.K. Gomma, M.H. Wahdan, Mater. Chem. Phys. 39 (1995) 209–213.
[60] A.K. Singh, M.A. Quraishi, Corros. Sci. 52 (2010) 1529–1535
[61] V.R. Saliyan, A.V. Adhikari, Bull. Mater. Sci. 31 (4) (2008) 699–711.
[62] R.F.V. Villamil, P. Corio, J.C. Rubin, S.M.L. Agostinho, J. Electroanal. Chem 535 (2002) 75–83.
[63] L. Yang, X. Li, G. Mu, Appl. Surf. Sci. 253 (2006) 2367–2372.
[64] A. K. Singh, J. Gopal, R. Prakash, E.E. Ebenso, A.K. Singh, Inter. J. Electrochem. Sci. 8 (2013) 9442–9448.
[65] M. Lebrini, M. Traisnel, M. Lagrenée, B. Mernari, F. Bentiss, Corros. Sci. 50 (2007) 473–479.
[66] Emranuzzaman, T. Kumar, S. Vishwanatham, G. Udayabhanu, Corros. Eng. Sci. Technol. 39, (2004) 327–332.
[67] N.M. Mallikarjuna, J. Keshavayya, B.M. Prasanna, B.M. Praveen, H.C. Tandon, J. Bio-Tribo-Corros. 6, Article number: 9 (2020).
[68] B.G. Ateya, B.E. El-Anadouli, F.M. El-Nizamy, Corros. Sci. 24 (1984) 509–515.
[69] M. Bouklah, B. Hammouti, M. Lagrenée, F. Bentiss, Corros. Sci. 48 (2006) 2831–2842.
[70] X. Li, S. Deng, G. Mu, H. Fu, F. Yang, Corros. Sci. 50 (2008)420–430.
[71] E. Kamis, F. Bellucci, R.M. Latanision, E.S.H. El-Ashry, Corrosion 47 (1991)677–686.
[72] M. El Faydy, R. Touir, M. Ebn Touhami, A. Zarrouk, C. Jama, B. Lakhrissi, L.O. Olasunkanmi, E.E. Ebenso, F. Bentiss, Phys. Chem. Chem. Phys. 20 (2018) 20167–20187.
[73] G.P. Lopez, D.G. Castner, B.D. Ratner, Surf. Interf. Anal. 17 (1991) 267–272.
[74] E.T. Kang, K.G. Neoh, K.L. Tan, Phys. Rev. B 44 (1991) 10461–10469.
[75] F. Moulder, W.F. Stickle, P.E. Sobol, K.D. Bomben, in: J. Chastain (Ed.), Handbook of X-Ray Photoelectron Spectroscopy, Perkin-Elmer Corp., Minnesota, USA, 1995.
[76] A.R. González-Elipe, A. Martínez-Alonso, J.M.D. Tascón, Surf. Interface Anal. 12 (1988) 565−571.
[77] W. Temesghen, P.M.A. Sherwood, Anal. Bioanal. Chem. 373 (2002) 601–608.

[78] K. Babić-Samardžija, C. Lupu, N. Hackerman, A.R. Barron, A. Luttge, Langmuir 21 (2005) 12187–12196.
[79] M. Bouanis, M. Tourabi, A. Nyassi, A. Zarrouk, C. Jama, F. Bentiss, Appl. Surf. Sci. 389 (2016) 952–966.
[80] P. Mourya, P. Singh, A.K. Tewari, R.B. Rastogi, M.M. Singh, Corros. Sci. 95 (2015) 71–87.
[81] M. Outirite, M. Lagrenée, M. Lebrini, M. Traisnel, C. Jama, H. Vezin, F. Bentiss, Electrochim. Acta 55 (2010) 1670–1681.
[82] V.S. Sastri, M. Elboujdaini, J.R. Rown, J.R. Perumareddi, Corrosion 52 (1996) 447–452.
[83] L. Reznik, L. Sathler, M. Cardoso, M. Albuquerque, Mater. Corros. 59 (2008) 685-690.
[84] A. El yaktini, A. Lachiri, M. El Faydy, F. Benhiba, H. Zarrok, M. El Azzouzi, M. Zertoubi, M. Azzi, B. Lakhrissi, A. Zarrouk, Int. J. Corros. Scale Inhib. 7 (2017) 609–632.
[85] S.K. Saha, A. Dutta, P. Ghosh, D. Sukul, P. Banerjee, Phys. Chem. Chem. Phys. 18 (2016) 17898–17911.
[86] R. Hsissou, F. Benhiba, M. Khudhair, M. Berradi, A. Mahsoune, H. Oudda, A. El Harfi, I.B. Obot, A. Zarrouk, J. King Saud Univ. Sci. 32 (2020) 667–676.
[87] C. Verma, Lukman O. Olasunkanmi, I.B. Obot, Eno E. Ebenso, M.A. Quraishi, RSC Adv. 6 (2016) 53933.
[88] L.O. Olasunkanmi, I.B. Obot, M.M. Kabanda, E.E. Ebenso, J. Phys. Chem. C 119 (2015) 16004–16019.
[89] R. Hsissou, F. Benhiba, S. Abbout. O. Dagdag. S. Benkhaya. Avni. Berisha. H. Erramli. A. Elharfi, J. Inorg. Chem. Commun. 115 (2020) 107858.
[90] F. Benhiba, Z. Benzekri, A. Guenbour, M. Tabyaoui, A. Bellaouchou, S. Boukhris, H. Oudda, I. Warad, A. Zarrouk, Chin. J. Chem. Eng. 28 (2020) 1436–1458.
[91] J. Haque, C. Verma, V. Srivastava, M.A. Quraishi, E.E. Ebenso, Results Phys. 9 (2018) 1481–1493.
[92] MarvinSketch Software, Version: 18.22, ChemAxon Ltd., 2018.
[93] A. El yaktini, A. Lachiri, M. El Faydy, F. Benhiba, H. Zarrok, M. El Azzouzi, M. Zertoubi, M. Azzi, B. Lakhrissi, A. Zarrouk, Orient. J. Chem. 34 (2018) 3016–3029.
[94] R. Nabah, F. Benhiba, Y. Ramli, M. Ouakki, M. Cherkaoui, H. Oudda, R. Touir, I. Warad, A. Zarrouk, J. Anal. Bioanal. Electrochem. 10 (2018) 1375–1398.
[95] Z. Muskalski, S. Wiewiorowska, Procedia Manuf. 2 (2015) 181–185.
[96] E. Ech-chihbi, A. Nahlé, R. Salim, H. Oudda, F. El Hajjaji, F. El Kalai, A. El Aatiaoui, M. Taleb, J. Bio. Tribo. Corros. 5 (2019) 24.
[97 E. Alibakhshi, M. Ramezanzadeh, G. Bahlakeh, B. Ramezanzadeh, M. Mahdavian, M. Motamedi, J. Mol. Liq. 255 (2018) 185–198.
[98] H. Rahmani, K.I. Alaoui, M. El Azzouzi, F. Benhiba, A. El Hallaoui, Z. Rais, M. Taleb, A. Saady, B. Labriti, A. Aouniti, A. Zarrouk, J. Chem. Data Collect. 24 (2019) 100302.
[99] M.E. Belghiti, S. Echihi, A. Mahsoune, Y. Karzazi, A. Aboulmouhajir, A. Dafali, I. Bahadur, J. Mol. Liq. 261 (2018) 62–75.
[100] J. Saranya, F. Benhiba, N. Anusuya, A. Zarrouk, S. Chitra, J. Chem. Data Collect. 26 (2020) 100358.
[101] G. Bahlakeh, A. Dehghani, B. Ramezanzadeh, M. Ramezanzadeh, J. Mol. Liq. 293 (2019) 111559.
[102] M. Murmu, S.K. Saha, N.C. Murmu, P. Banerjee, Corros. Sci. 146 (2019) 134–151.
[103] R. Hsissou, F. Benhiba, O. Dagdag, M. El Bouchti, K. Nouneh, M. Assouag, S. Briche, A. Zarrouk, A. Elharfi, J. Colloid Interf. Sci. 574 (2020) 43–60.
[104] M. Rbaa, F. Benhiba, A.S. Abousalem, M. Galai, Z. Rouifi, H. Oudda, B. Lakhrissi, I. Warad, A. Zarrouk, J. Mol. Struct. 1213 (2020) 128155.

Graphical abstract

Inhibitor molecule

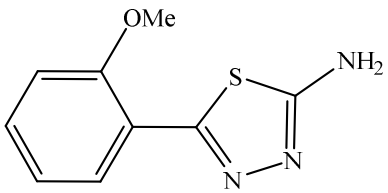

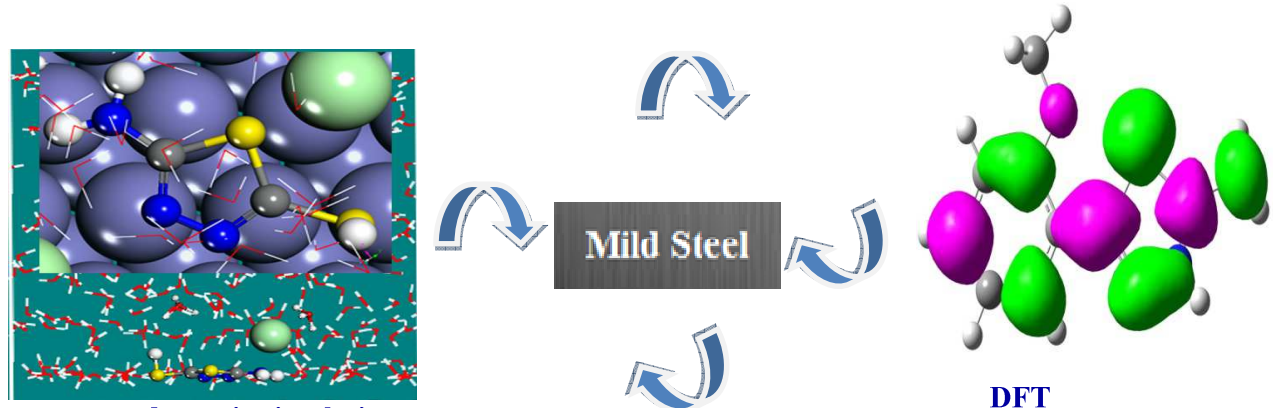

Molecular dynamic simulation

DFT

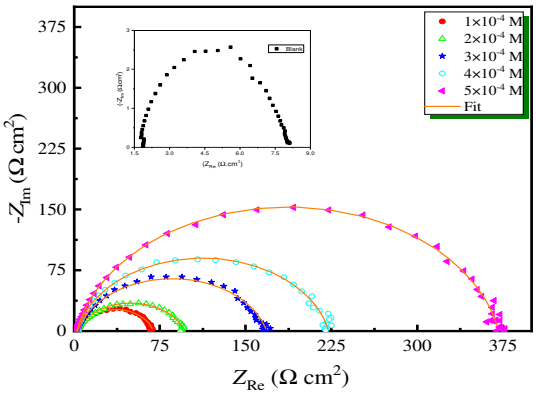

EIS study

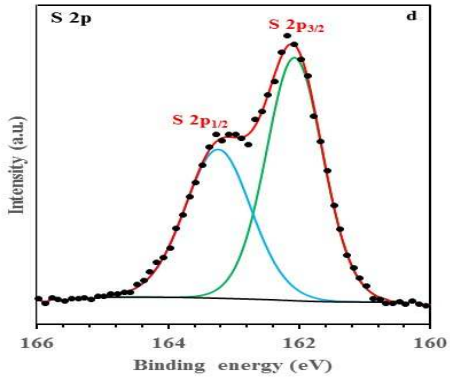

XPS